

**Maintenance of
Arctic stratocumulus**

A. Solomon et al.

Moisture and dynamical interactions maintaining decoupled Arctic mixed-phase stratocumulus in the presence of a humidity inversion

A. Solomon^{1,2}, M. D. Shupe^{1,2}, P. O. G. Persson^{1,2}, and H. Morrison³

¹CIRES, University of Colorado, Boulder, CO, USA

²Earth System Research Laboratory/NOAA, Boulder, CO, USA

³MMM/NESL/NCAR, Boulder, CO, USA

Received: 20 April 2011 – Accepted: 23 April 2011 – Published: 4 May 2011

Correspondence to: A. Solomon (amy.solomon@noaa.gov)

Published by Copernicus Publications on behalf of the European Geosciences Union.

Title Page

Abstract

Introduction

Conclusions

References

Tables

Figures

◀

▶

◀

▶

Back

Close

Full Screen / Esc

Printer-friendly Version

Interactive Discussion



Abstract

Observations suggest that processes maintaining subtropical and Arctic stratocumulus differ, due to the different environments in which they occur. For example, specific humidity inversions (specific humidity increasing with height) are frequently observed to occur coincident with temperature inversions in the Arctic, while they do not occur in the subtropics. In this study we use nested LES simulations of decoupled Arctic Mixed-Phase Stratocumulus (AMPS) clouds observed during the DOE Atmospheric Radiation Measurement Program's Indirect and SemiDirect Aerosol Campaign (ISDAC) to analyze budgets of water components, potential temperature, and turbulent kinetic energy. These analyses quantify the processes that maintain decoupled AMPS, including the role of the humidity inversions. The results show the maintenance of liquid clouds in both the shallow upper entrainment zone (temperature and humidity inversion) due to a down gradient transport of water vapor by turbulent fluxes into the cloud layer and direct condensation by radiative cooling, and in the updrafts of the mixed-layer eddies below cloud top due to buoyant destabilization. These processes cause at least 20 % of the cloud liquid water to extend into the inversion. The redistribution of water vapor from the top of the humidity inversion to the base of the humidity inversion maintains the cloud layer while the mixed layer-entrainment zone system is continually losing total water. In this decoupled system, the humidity inversion is the only source of water vapor for the cloud system since water vapor from the surface layer is not efficiently transported into the mixed layer. Sedimentation of ice is the dominant sink of moisture from the mixed layer.

1 Introduction

Arctic mixed-phase stratocumulus (AMPS) are observed to occur approximately 45 % of the time on the North Slope of Alaska, with a significant increase in occurrence during the spring and fall transition seasons (Shupe, 2011). Due to the presence of

ACPD

11, 13469–13524, 2011

Maintenance of Arctic stratocumulus

A. Solomon et al.

Title Page

Abstract

Introduction

Conclusions

References

Tables

Figures

◀

▶

◀

▶

Back

Close

Full Screen / Esc

Printer-friendly Version

Interactive Discussion



Maintenance of Arctic stratocumulus

A. Solomon et al.

Title Page

Abstract

Introduction

Conclusions

References

Tables

Figures

◀

▶

◀

▶

Back

Close

Full Screen / Esc

Printer-friendly Version

Interactive Discussion



liquid water in these clouds, they play an important role in the structure of the Arctic atmospheric boundary layer (ABL) and surface energy budget. For example, Morrison and Pinto (2006) demonstrated that, in mesoscale simulations of a springtime Surface Heat Budget of the Arctic Ocean (SHEBA) case study in the Beaufort Sea area, it is necessary to adequately simulate AMPS to produce well-mixed ABLs. In addition, since cloud liquid water causes an increase in downwelling longwave radiation and a decrease in incoming shortwave radiation, inadequate simulations of Arctic clouds cause significant errors in the modeled surface energy budget (e.g., Curry et al., 2000; Solomon et al., 2009).

AMPS are typically observed to persist for days in both the spring, when the Arctic Ocean is essentially ice covered, and fall, when the open ocean produces large fluxes of heat and moisture into the atmospheric boundary layer (see Shupe et al., 2006; Shupe, 2011). The persistence of AMPS under both strong and weak surface forcing conditions suggests that other mechanisms also contribute to the maintenance of these clouds, and that the relative contributions by the mechanisms may differ from spring to fall. This idea is supported by mesoscale model simulations of AMPS observed during the fall Mixed-Phase Arctic Cloud Experiment (MPACE, Morrison et al., 2008), where liquid water paths (LWPs) in AMPS during periods of open water were found to be less sensitive to changes in cloud condensation nuclei (CCN) than for clouds in modeling studies over sea ice (e.g., Pinto, 1998; Harrington et al., 1999; Jiang et al., 2001). In addition, the Morrison et al. MPACE study found that changes in LWP did not significantly impact the large-scale circulation, in contrast to modeling studies of ice-covered conditions during SHEBA (Morrison and Pinto, 2006). However, AMPS forcing mechanisms involving cloud-top processes are likely relatively insensitive to seasonal differences of surface characteristics. In cases with and without open water, Pinto (1998) observed entrainment of air aloft by turbulent mixing, and downdrafts in the boundary layer were forced by cloud top radiative cooling.

AMPS have not been studied as extensively as stratocumuli that occur in regions of the descending branch of the Hadley circulation over relatively cool subtropical oceans

Maintenance of Arctic stratocumulus

A. Solomon et al.

Title Page

Abstract

Introduction

Conclusions

References

Tables

Figures

◀

▶

◀

▶

Back

Close

Full Screen / Esc

Printer-friendly Version

Interactive Discussion



(Sc) (Norris 1998). Observations indicate that the processes that maintain subtropical and Arctic stratocumulus differ, due to the different environments in which they occur. For example, specific humidity inversions (specific humidity increasing with height) are frequently observed to occur coincident with temperature inversions in the Arctic (e.g., Curry et al., 1996; Tjernström et al., 2004; Sedlar and Tjernström, 2009). In a recent study, Sedlar et al. (2011) surveyed data from SHEBA, the Arctic Summer Cloud Ocean Study (ASCOS) in the central Arctic Basin, and at Barrow, Alaska, to find that specific humidity inversions occurred 75–80 % of the time when low-level clouds were present. In addition, this study found a significant relationship between the existence of specific humidity inversions and AMPS that extended into the temperature inversion, highlighting the difference between AMPS and subtropical stratocumulus where the entrainment of dry air aloft prevents cloud liquid water from forming in the temperature inversion. Other important differences between warm Sc and AMPS are more effective cloud top radiative cooling because of the cold, dry overlying Arctic free troposphere, and the vapor diffusion onto ice (Bergeron process) which acts as a potentially large sink of water vapor for AMPS even when there is limited liquid water. In warm Sc, drizzle grows by collision-coalescence of droplets, so as liquid water decreases, drizzle will shut off (see Morrison et al., 2011 for a detailed discussion of this point).

To highlight the differences between Arctic and subtropical stratocumulus, we first plot fields from a sounding taken during the springtime over Graciosa Island in the Azores of a single layer stratocumulus deck (Fig. 1). This subtropical sounding indicates an inversion of 5 K at 2.2 km. A decrease in specific humidity with height causes the equivalent potential temperature (θ_e) to also decrease with height, most significantly near the surface, at the base of the subcloud layer, and within the inversion. A sharp decrease in humidity causes the inversion to be potentially unstable by the Cloud Top Entrainment Instability (CTEI) criteria (e.g., Randall, 1980; Deardorff, 1980) between 0.5 km and 1.5 km. Longwave cooling at cloud top at 2.15 km causes the sharp, strong inversion, caps the cloud layer and limits the entrainment of warm, dry air from above (e.g., Nichols, 1984). In addition, horizontal winds indicate divergence that

is approximately constant with height within the mixed layer that balances the large-scale subsidence above cloud top (not shown). These conditions are typical of marine stratocumulus-topped boundary layers. For example, see composites in Albrecht et al. (1995) and Norris (1998).

5 There have been many studies of decoupling in subtropical Sc. The decoupling of the warm moist surface air from the cloud layer in the subtropical sounding is due to the warming of the cloud layer by the absorption of solar radiation, which limits the extent of the mixing by turbulence generated by longwave cooling within the cloud layer (e.g., Nichols 1984). However, decoupling can also occur due to the evaporation of drizzle
10 below the subcloud layer (e.g., Brost et al., 1982) and the advection of the Sc cloud deck over warmer SSTs (e.g., Wyant et al., 1997). Decoupling in subtropical Sc can cause the cloud to evaporate unless cumulus clouds form below the subcloud layer and transport moisture upward to the cloud layer (Nicholls, 1984).

15 Idealized model studies have been used to study the impact of precipitation on subtropical Sc. Specifically, sedimentation causes a decrease in cloud water in the entrainment zone, decreasing longwave cooling and turbulent mixing of dry warm air aloft into the cloud layer, ultimately increasing the liquid water path (e.g., Ackerman et al., 2004; Bretherton et al., 2007). Drizzle stabilizes the boundary layer by latent heating in the cloud layer and evaporation below cloud base, potentially depleting the boundary
20 layer of water if the drizzle is strong enough to reach the surface (e.g., Stevens et al., 1998).

25 A sounding showing a single layer Arctic mixed-phase stratocumulus-topped boundary layer is plotted in Fig. 5a. This sounding was taken in the springtime when the Arctic Ocean was essentially ice-covered. However, satellite images indicate that there were regions of open water providing a source of low-level moisture. A detailed discussion of this Arctic case study is provided in Sect. 2. The sounding indicates a surface temperature of $\sim -8^{\circ}\text{C}$ and specific humidity of $\sim 1.7\text{ g kg}^{-1}$. The θ_e profile monotonically increases with height by 1.5 K up to 500 m where the slope changes sharply, indicating a decoupling between the stable surface layer and the subcloud layer (a well-

Maintenance of Arctic stratocumulusA. Solomon et al.

[Title Page](#)[Abstract](#)[Introduction](#)[Conclusions](#)[References](#)[Tables](#)[Figures](#)[◀](#)[▶](#)[◀](#)[▶](#)[Back](#)[Close](#)[Full Screen / Esc](#)[Printer-friendly Version](#)[Interactive Discussion](#)

5 mixed layer between 0.5–1.1 km) and a cloud top that is stable relative to the overlying atmosphere. The temperature profile indicates an inversion of 5 K at 1.1 km with an entrainment zone of approximately 40 m. In this study we estimate the boundaries of entrainment zones by discontinuities in the slope of equivalent potential temperature, which yields similar results to assuming the top of the entrainment zone is located at the top of a region of negative buoyancy in our model studies (see Deardorff, 1979 for a discussion on this point). The specific humidity profile indicates a decrease with height from the surface to the base of the temperature inversion, with a humidity inversion coincident with the temperature inversion, suggesting the horizontal advection of warm, moist air aloft. Specific humidity at the top of the inversion is approximately equal to humidity at the surface. Horizontal winds indicate significant shear at the inversion (similar to observations of Sc off the coast of California, e.g., Albrecht et al., 1985), the base of the subcloud layer, and near the surface. Winds are relatively weak within the mixed layer.

15 The role of precipitation in decoupled AMPS is an open area of research, since it is unclear how the existence of ice in these clouds changes the conceptual model of subtropical Sc developed from idealized mixed-layer model and LES studies. We focus our study on decoupled conditions in AMPS in order to focus on the conditions that make AMPS distinct from subtropical Sc. Specifically, we focus on quantifying the role of humidity inversions at cloud top in the maintenance of AMPS.

20 In this study we present results from nested LES simulations of AMPS during the DOE Atmospheric Radiation Measurement (ARM) Program's Indirect and SemiDirect Aerosol Campaign (ISDAC, McFarquhar et al., 2011). In Sect. 2 we outline observations of the environmental conditions and cloud properties during ISDAC. In Sect. 3 we describe the model and experiment design. In Sect. 4 we validate the model results by comparisons with retrievals and soundings taken at Barrow, Alaska. In Sect. 5 we present budgets of cloud water (q_c), cloud ice (q_i), water vapor (q_v), total water (q_t), potential temperature (θ), and turbulent kinetic energy (TKE) to quantify the processes that maintain the AMPS. In Sect. 6 we discuss our findings relative to previous studies

Maintenance of Arctic stratocumulus

A. Solomon et al.

[Title Page](#)[Abstract](#)[Introduction](#)[Conclusions](#)[References](#)[Tables](#)[Figures](#)[◀](#)[▶](#)[◀](#)[▶](#)[Back](#)[Close](#)[Full Screen / Esc](#)[Printer-friendly Version](#)[Interactive Discussion](#)

of Arctic and subtropical stratocumulus clouds.

2 Observations

2.1 Synoptic-scale features

In April 2008, ISDAC was carried out to measure mixed-phase clouds for both clean and polluted environments (see McFarquhar et al., 2011). Two “golden days” were identified where single-layer mixed phase stratocumulus were observed and extensively measured by aircraft and ground-based sensors. This study focuses on the “golden day” of 8 April 2008, when a single layer stratocumulus deck was observed over the North Slope of Alaska. During the period of this study, the Beaufort Sea was generally ice covered and roll clouds were not observed, in contrast to fall conditions (for example, see MPACE case study of Solomon et al., 2009). However, visible images taken on 8 April by the Terra satellite indicate that significant areas of open water east of Barrow may have impacted cloud formation and boundary layer structure during this period. Two soundings were taken at Barrow on the 8th at 4.4 Z and 17.6 Z (see Fig. 5a). These soundings indicate that during 1–6 Z, the wind direction was northerly at the surface, gradually transitioning to easterly at 1.4 km. The winds shifted to east-southeasterly as a high pressure system passed over Barrow moving northwestward at 8 Z.

2.2 Cloud and boundary layer properties

At Barrow, measurements taken with a ground-based vertically pointing 35-GHz cloud radar, a micropulse cloud lidar, and a dual-channel microwave radiometer were combined (Shupe, 2007) to reveal multi-layered mixed-phase and ice clouds extending from the surface to 3 km that persisted from 0 Z–8 Z until a warm front moved in and the cloud top descended to 1 km. At 8 Z, the interpolated temperature profile shows

Maintenance of Arctic stratocumulus

A. Solomon et al.

Title Page

Abstract

Introduction

Conclusions

References

Tables

Figures

◀

▶

◀

▶

Back

Close

Full Screen / Esc

Printer-friendly Version

Interactive Discussion



Maintenance of Arctic stratocumulus

A. Solomon et al.

[Title Page](#)[Abstract](#)[Introduction](#)[Conclusions](#)[References](#)[Tables](#)[Figures](#)[◀](#)[▶](#)[◀](#)[▶](#)[Back](#)[Close](#)[Full Screen / Esc](#)[Printer-friendly Version](#)[Interactive Discussion](#)

a sharp (~ 3 K) inversion at ~ 1 km, with AMPS near the base and up into the inversion by approximately 100 m (Fig. 2a). The AMPS persisted until 12 Z 9 April and slowly descended from 1 km to 500 m over this period. Ice precipitated from the base of the AMPS but only trace precipitation was observed at the surface near Barrow. Indications of a secondary cloud layer were observed at 10, 12, and 16 Z. The sounding at 17.6 Z (Fig. 5a) indicates that the surface and cloud layer were decoupled, with a well-mixed layer at cloud base (static stabilities close to neutral, $\partial\theta/\partial z \cong 0$) and a stable layer below (static stabilities greater than 2 K/km below 500 m layer). Water vapor mixing ratios decreased from 1.7 g kg^{-1} at the surface to 1.2 g kg^{-1} at cloud top above which a secondary maximum of 1.6 g kg^{-1} was observed.

Microphysical properties for these clouds were also derived from the ground-based remote sensors. First, the cloud phase classification of Shupe (2007) was used to determine the vertical distribution of cloud phase. Then, cloud ice water content, and its vertical integral the ice water path (IWP), were derived from cloud radar reflectivity measurements with an uncertainty of up to a factor of two (Shupe et al., 2006). Cloud liquid water path (LWP) was derived from dual-channel microwave radiometer measurements with an uncertainty of 20–30 g m^{-2} (Turner et al., 2007). Finally, in-cloud vertical air velocity (w) was derived from cloud radar Doppler spectra (Shupe et al., 2008a). Between 12–24 Z, IWP exceeded LWP and the liquid fraction (LF, ratio of LWP to LWP+IWP) was generally below 0.4. IWP generally exceeded 60 g m^{-2} and LWP ranged between 20–100 g m^{-2} . IWP and LWP were significantly correlated over 2 min to 1 h averaging periods (results not shown). Unlike AMPS observed during the fall at Barrow, IWP was not depleted in downdrafts (see Shupe et al., 2008b). The cloud-averaged w , LWP, and IWP had maximum correlations at zero lag (results not shown).

3 Model setup and experiment design

3.1 WRF V3.1

The Weather Research Forecast (WRF) V3.1 model (Skamarock et al., 2008) is used for this study with five two-way nested grids with horizontal grid spacings of 25 km, 5 km, 1 km, 200 m, and 50 m (Fig. 3). The 50 m nest has 241 × 241 horizontal gridpoints (12 km × 12 km) and is placed just to the northwest of Barrow. The boundary layer is well resolved in the vertical by including 85 pressure levels below 800 hPa. In order to better resolve entrainment and mixing in the mixed-layer and entrainment zone, $\Delta z = 16$ m in the mixed layer (0.6–1.5 km) with Δz decreased to 8 m in the entrainment zone (1.2–1.4 km). Below 0.6 km and above 1.5 km $\Delta z = 50$ m. Second order diffusion with a 1.5 order TKE prediction scheme is used to parameterize subgrid turbulence in the 1 km, 200 m and 50 m nests. The model is forced with lateral and surface boundary conditions from the European Centre for Medium-Range Weather Forecasts' (ECMWF) 4× daily, T255 ERA-Interim dataset. The model is spun-up by integrating from 0 UTC 8 April to 12 Z UTC 8 April. The 200 m and 50 m nests are started at 18 Z and spun up by integrating for 2 h. The subsequent 90-min period 20:00–21:29 UTC 8 April is used in the analysis.

The radiation, surface layer, land surface, and planetary boundary layer options used in the model runs are described in Table 1. Ice is initiated by condensation freezing, aerosol freezing, contact freezing, and immersion freezing. Homogeneous freezing of cloud droplets is negligible for temperatures observed during ISDAC. The concentration of ice nuclei acting in deposition and condensation freezing modes is specified from observations using the continuous flow diffusion chamber from the MPACE campaign (Prenni et al., 2007). Cloud droplets are activated in regions of low cloud water content using the resolved and subgrid vertical motion (Morrison and Pinto, 2005) and a lognormal aerosol size distribution to derive the cloud condensation nuclei spectra following Abdul-Razzak and Ghan (2000). The log-normal dry aerosol size distribution was fit to in-situ measurement from the National Research Council of Canada

Maintenance of Arctic stratocumulus

A. Solomon et al.

Title Page

Abstract

Introduction

Conclusions

References

Tables

Figures

◀

▶

◀

▶

Back

Close

Full Screen / Esc

Printer-friendly Version

Interactive Discussion



Convair-580 (personal communication Peter Liu, Environment Canada) with a size distribution given by

$$\frac{dN}{d\ln r} = \frac{N_t}{\sqrt{2\pi}\ln\sigma} \exp\left\{-\frac{\ln^2(r/r_m)}{2\ln^2\sigma}\right\}, \quad (1)$$

where N is the number concentration of aerosols and r is the particle radius. The parameters N_t , r_m , and σ are total number concentration, geometric mean radius and standard deviation of each particle mode and are given the values 165 cm^{-3} , $1.3\text{ }\mu\text{m}$, and 1.4, respectively. Aerosol composition is assumed to be ammonium bisulphate with an insoluble fraction of 30 %.

The microphysical cloud scheme used in this study includes two-moments for cloud droplets, rain, ice, snow, and graupel. This means a prognostic equation for mixing ratio and number concentration is integrated for each of the 5-hydrometeor classes. Morrison et al. (2009) provide details of the parameterizations used in this microphysical scheme.

3.2 Experiment design

A significant amount of open water was observed during ISDAC along the eastern Alaskan coast. However, this modeling study is focused on the maintenance of decoupled stratocumulus. We therefore removed all regions of open water and set the ocean surface uniformly to sea ice. However, removing the open water had a negligible impact on the simulations presented in this study.

In this model study, WRF is run with high enough resolution to resolve the turbulent eddies that contain the most kinetic energy and transport the most heat and momentum, i.e. as a large eddy simulation (LES). However, different from traditional LESs, this study does not use periodic boundary conditions, where an eddy that is advected out one side of the domain enters through the other side of the domain. Rather, eddies from the 200 m nest are advected into the 50 m nest and variability with scales finer

Maintenance of Arctic stratocumulus

A. Solomon et al.

Title Page

Abstract

Introduction

Conclusions

References

Tables

Figures

◀

▶

◀

▶

Back

Close

Full Screen / Esc

Printer-friendly Version

Interactive Discussion



than 200 m evolve within the 50 m nest. This modeling strategy has been successfully applied to simulations of boundary layer clouds in heterogeneous conditions that are directly linked to synoptic systems (for example, see Zhu et al., 2010). In the 50 m nest, it takes approximately 1 km for the turbulent structures to spin up (results not shown).

In this study we analyze the budgets of quasi-conserved moist variables, such as θ_e and total water (q_t), as well as potential temperature (q) and turbulent kinetic energy (TKE) to understand the processes involved in the maintenance and persistence of observed springtime Arctic mixed phase stratocumulus (a complete list of symbols is provided in Table 2).

Equivalent potential temperature, θ_e , is equal to

$$\theta_e = \left(T + \frac{L}{c_p} q_v \right) \left(\frac{p_0}{p} \right)^{\frac{R}{c_p}} = \theta + \left(\frac{L}{c_p} q_v \right) \left(\frac{p_0}{p} \right)^{\frac{R}{c_p}} \quad (2)$$

The prognostic equations for q and water constituents are

$$\frac{\partial \theta}{\partial t} = \left(\frac{p_0}{p} \right)^{\frac{R}{c_p}} Q_1 - \mathbf{u} \cdot \nabla \theta - w \frac{\partial \theta}{\partial z} \quad (3)$$

$$\frac{\partial q_*}{\partial t} = Q_{2*} - \mathbf{u} \cdot \nabla q_* - w \frac{\partial q_*}{\partial z} \quad (4)$$

where Q_1 is diabatic heating and is composed of radiative heating (Q_r) and condensational heating/cooling (Q_c) and Q_{2*} is diabatic moistening due to phase changes. Sedimentation, or gravitational settling, is included in the Q_{2*} term. In Eq. (4) q_* can be vapor (q_v), liquid (q_c), ice + snow + graupel (q_i) or total water ($q_t = q_v + q_c + q_i$).

To separate mesoscale and turbulent variability, all turbulent fluxes are calculated with 15 min averaged fields. Fifteen minutes is approximately the time scale between mesoscale variability and the “energy-containing” scales in the retrieved vertical velocity spectra (results not shown). For example, for vertical fluxes, the turbulent vertical flux is, $\overline{w'q_*'} = \overline{wq_*} - \overline{w} \overline{q_*}$, where primes denote deviations from the temporal averages and overbars signify temporal averages over 15 min (equal to the average over 1800

Maintenance of Arctic stratocumulus

A. Solomon et al.

Title Page

Abstract

Introduction

Conclusions

References

Tables

Figures

◀

▶

◀

▶

Back

Close

Full Screen / Esc

Printer-friendly Version

Interactive Discussion



Discussion Paper | Discussion Paper | Discussion Paper | Discussion Paper | Discussion Paper

time steps). Vertical profiles are calculated by horizontally averaging (denoted with angled brackets) across a 6.5 km × 6.5 km square domain, 1 km away from horizontal boundaries. The budgets expressed in Eqs. (3)–(4) are also averaged over up-drafts and downdrafts separately to investigate the turbulent dynamics that maintain the mixed layer and cloud layer structures.

In a nearly horizontally homogenous system (where the length scale of the most energetic turbulent eddies is much smaller than the characteristic scale of the eddy correlations) the TKE-budget can be written as (see Garratt, 1992, p. 33, Eq. 2.74a):

$$\underbrace{\frac{\partial \bar{e}}{\partial t}}_E = \underbrace{\frac{g}{\theta_0} \overline{w' \theta'_v}}_B - \underbrace{\left(\overline{u' w'} \frac{\partial \bar{u}}{\partial z} + \overline{v' w'} \frac{\partial \bar{v}}{\partial z} \right)}_S - \underbrace{\frac{\partial \overline{w' e}}{\partial z}}_T - \underbrace{\frac{\partial \overline{w' p'}}{\rho \partial z}}_P - \underbrace{\varepsilon}_D \quad (5a)$$

$$\text{Where } e = 0.5(\overline{u' u'} + \overline{v' v'} + \overline{w' w'}), \quad (5b)$$

$$\theta_e = \theta(1 + 0.61 q_v - q_i - q_c), \quad (5c)$$

$$\text{and buoyancy flux} = \overline{w' \theta'_v}. \quad (5d)$$

The term E is storage, the term B is buoyancy production, the term S is shear production, the term T is turbulent vertical transport, the term P is pressure transport and D is viscous dissipation.

4 Validation of 1 km nest at Barrow

The model simulates the vertical extent and ice water content (IWC) of the predominantly ice cloud that was observed between 0–8 Z (results not shown). The model also simulates the mixed phase stratocumulus that was observed starting at 8 Z, with maximum liquid water content (LWC) at 1.3 km, and the slow descent of the cloud from 8 Z 8 April to 12 Z 9 April (Fig. 2). At times multiple layers of liquid are produced within the model, consistent with the ground-based observations. Modeled IWC in the AMPS

Maintenance of Arctic stratocumulus

A. Solomon et al.

Title Page

Abstract

Introduction

Conclusions

References

Tables

Figures

◀

▶

◀

▶

Back

Close

Full Screen / Esc

Printer-friendly Version

Interactive Discussion



is underestimated by a factor of 3–4, a difference that is larger than the expected uncertainty in derived IWC. However, qualitatively, the model does tend to show a relative increase in IWC in a layer near the surface, which is again consistent with the radar-derived IWC profiles. The 1 km, 200 m, and 50 m nests produce AMPS with equivalent structure and magnitude (figure not shown). Cold temperatures aloft (estimated from the soundings) descend more slowly in the simulation causing a single layer AMPS to form at 1.2 km from 18–22 Z, while retrievals show cloud tops closer to 800 m at this time.

In Fig. 4 we compare w , LWP, and IWP power spectra at Barrow for the 2-h period 20–22 Z from the retrievals, the 1 km nest and the 50 m nest (50 m nest values are taken to the west of Barrow at 71.33° N, 156.91° W). The w time series used in this analysis are vertical averages over the layer containing cloud liquid water, as vertical velocity structures were typically vertically coherent in nature. Looking at the w spectra first, the 50 m nest is reproducing the variability well into the inertial sub-range ($\nu > \sim 0.01 \text{ s}^{-1}$), while the 1 km nest can only resolve time scales longer than $\sim 10 \text{ min}$ ($\nu < \sim 2 \times 10^{-3} \text{ s}^{-1}$), which is consistent with the 7 m s^{-1} horizontal wind speed and a $4\Delta x$ resolution. It is interesting to note that the 1 km nest can simulate similar coarse-scale variability and structure as the 50 m nest despite not resolving small scales. Similar results are seen for the LWP; both the 50 m and 1 km nest have similar variability on the 10–20 min time scale while only the 50 m resolves the finer scale variability. The spectra for the IWP show that the 50 m nest is underestimating the variability in small scales, even though these scales are better simulated in the LWP and w spectra, suggesting difficulties with initiation and/or growth of cloud ice and snow in the model.

Maintenance of Arctic stratocumulus

A. Solomon et al.

[Title Page](#)[Abstract](#)[Introduction](#)[Conclusions](#)[References](#)[Tables](#)[Figures](#)[I◀](#)[▶I](#)[◀](#)[▶](#)[Back](#)[Close](#)[Full Screen / Esc](#)[Printer-friendly Version](#)[Interactive Discussion](#)

5 Nested LES simulations

5.1 Comparison with a sounding at Barrow

In this study we focus our analysis on the single layer AMPS that persisted from 18–22 Z in the model. In Fig. 5, we compare the environmental conditions to the west of Barrow at 20 Z in the 50 m nest (hereafter referred to as the LES) to the nearest-in-time sounding taken at Barrow at 17.6 Z. Note that these vertical profiles are for different times at different locations since cloud structure in the model similar to the sounding occurs slightly later and this study focuses on the region to the west of Barrow with uniform surface conditions. The red star in Fig. 6 shows the location of the vertical profiles plotted in Fig. 5b. A well-mixed surface layer and cloud layer is seen in the LES; however, the LES has a deeper stable layer between the surface and cloud layer than observed. The simulated temperature inversion strength of 6.5 K is slightly greater than the observed 5 K inversion; however, the simulated humidity inversion of 0.45 g kg^{-1} is slightly weaker than observed. The cloud liquid water maximum is at the base of the humidity inversion, and cloud water extends into the temperature inversion by approximately 100 m in both the LES and sounding. On average, 23 % of the simulated cloud liquid water is located within the inversion. Observations are unable to determine the amount of liquid water below versus above the inversion base. Observed winds indicate shear in the surface layer and weaker winds within the cloud and sub-cloud layer. While qualitatively similar in many regards, the LES shows larger shear at cloud top; part of this difference may be due to vertical smoothing of the radiosonde measurements during data acquisition.

5.2 Vertical structure along mean wind in cloud layer

The spatial distribution of LWP in the LES at 20 Z is plotted in Fig. 6. The square in the figure marks a region that is 1.5 km away from any boundary and consistently has single layer AMPS with cloud tops at $\sim 1.3 \text{ km}$ for the 20–22 Z period (a front that

Maintenance of Arctic stratocumulus

A. Solomon et al.

Title Page

Abstract

Introduction

Conclusions

References

Tables

Figures

◀

▶

◀

▶

Back

Close

Full Screen / Esc

Printer-friendly Version

Interactive Discussion



Maintenance of Arctic stratocumulus

A. Solomon et al.

Title Page

Abstract

Introduction

Conclusions

References

Tables

Figures

◀

▶

◀

▶

Back

Close

Full Screen / Esc

Printer-friendly Version

Interactive Discussion



moves in from the east at the end of the period causes cloud top to descend in the area to the northeast of this square). This region is used for statistics discussed in the following sections. Figure 7 shows the vertical structure of various fields along the red dashed line in Fig. 6, which is approximately parallel to the mean winds in the cloud layer. This figure depicts a single layer cloud with cloud top at ~ 1.3 km and cloud base at ~ 1 km, with cloud water extending into the inversion by about 50 m. The inversion base is at 1250 m. Cloud ice forms within the liquid cloud layer (Fig. 7b), sometimes very near the top, and precipitates below the cloud layer. The precipitating ice sublimates to some degree in a dry layer below the cloud, but tends to grow again in the relatively moist surface layer. Characteristic subgrid vertical velocity is estimated from the predicted subgrid turbulent kinetic energy, assuming isentropic turbulence ($w' = u' = v'$), as $w' = (2/3TKE)^{1/2}$. Subgrid vertical velocity is seen in three physically distinct regions: at the inversion top, in a layer encompassing the cloud and sub-cloud, and near the surface (Fig. 7c). The magnitude of the subgrid vertical velocity in the mixed layer is $\sim 4\times$ smaller than the resolved vertical velocity but clearly significant. Resolved downdrafts (Fig. 7d) are stronger and narrower than the updrafts, consistent with generation by cloud-top cooling. The strongest vertical motions are generally confined to the cloud layer itself. Small-scale variability is seen within and above the inversion. Generally weak vertical motions also occur below 0.7 km.

Figure 7e,f shows q_e and total water (q_t) along the diagonal slice. Since these two fields are quasi-conserved during adiabatic changes including vapor–liquid phase changes (θ_e is not conserved during liquid–ice phase changes), they are commonly used to identify mixed-layer structure and define idealized mixed-layer models. A well-mixed cloud and subcloud layer is seen in Fig. 7e,f to extend from the base of the inversion to 800 m. Total water maxima are seen at and above the inversion and at the surface, with a region of drier air below the mixed layer. Small-scale fluctuations penetrating the interfaces at the top and bottom of the mixed layer are clearly seen in Fig. 7e,f. The role of these fluctuations in maintaining the mixed layer is described in the next section.

5.3 Total domain averages

5.3.1 Buoyancy fluxes

Figure 8 shows the vertical buoyancy fluxes, $\overline{w'\theta'_v}$, and θ_e averaged temporally over 90 min and horizontally over the square domain in Fig. 6. Positive buoyancy flux occurs in the mixed layer and near the surface. Weak negative buoyancy flux is present between these two layers. The cloud top is capped by a layer of negative buoyancy flux associated with the damping effect of the temperature inversion. Motions in regions with positive buoyancy flux are stabilizing, producing TKE at the expense of potential energy. Motions in regions with negative buoyancy flux are destabilizing, reducing TKE to produce potential energy. Note that the cloud top actually resides in a region of negative buoyancy flux. The small difference between the buoyancy flux and the potential temperature flux ($\overline{w'\theta'}$, red curves) indicates that water variations are making a negligible contribution to the buoyancy flux.

Figures 8b and c are the same curves as in Fig. 8a enlarged in the region of the upper entrainment zone (Fig. 8b) and the lower entrainment zone (Fig. 8c). The dash-dot gray lines indicate the θ_e slopes in the mixed layer and the \sim dry adiabatic lapse rate above (below) the upper (lower) entrainment zones. The depth of the entrainment zones is estimated as the region where the slope of θ_e deviates from the constant slopes marked with the gray dash-dot lines; specifically, 1.24–1.3 km (depth = 60 m) for the entrainment zone at cloud top and 0.62–0.82 km (depth = 200 m) for the entrainment zone at the base of the mixed layer. Therefore, the θ_e profile indicates that there are effectively two mixed-layers, one being the actual boundary layer near the surface up to about 400 m and the other being the cloud-driven mixed-layer. Thus, the cloud is decoupled from the surface and thus not deriving much (or any) of its energy from surface forcing.

Maintenance of Arctic stratocumulus

A. Solomon et al.

Title Page

Abstract

Introduction

Conclusions

References

Tables

Figures

◀

▶

◀

▶

Back

Close

Full Screen / Esc

Printer-friendly Version

Interactive Discussion



5.3.2 Potential temperature tendencies

Negative potential temperature fluxes (buoyancy fluxes) due to entrainment forced by radiative cooling are seen to extend throughout the inversion with peak fluxes occurring at 1.27 km, 30 m above the top of the mixed layer (Fig. 8a). Positive potential temperature fluxes extend from 0.9 km to the top of the mixed layer, peaking at 1.18 km. The divergence of potential temperature fluxes between 1.27–1.35 km produce cooling. The convergence of potential temperature fluxes between 1.18–1.27 km, a warming effect, largely balances the radiative cooling plus condensational heating in the upper 60 m of the cloud layer (Fig. 9a). Longwave cooling dominates over the warming tendencies causing the net tendency to be a cooling of -5 to -30 K day^{-1} in the upper entrainment zone (Fig. 9a). The convergence of potential temperature fluxes from 1.18–1.27 km is due to entrainment of sensible heat within and above the temperature inversion. As seen in Fig. 9a, the longwave cooling peaks in the inversion (entrainment zone) but extends 80 m into the mixed layer, coincident with and offset by turbulent vertical potential temperature fluxes (ADV term in Fig. 9a). The average potential temperature tendency due to longwave cooling at the top of the mixed layer is approximately -80 K day^{-1} . Fluxes due to the mean flow are significant at the top of the upper entrainment zone, where potential temperature tendencies due to both the horizontal and vertical flow exceed 30 K day^{-1} (results not shown). However, there is large variability within the upper entrainment zone with the standard deviation of 15 min horizontally and vertically averaged longwave cooling and advection equal to 2.9 K day^{-1} and 26.6 K day^{-1} , respectively. Averaged advection variability is primarily due to advection by the mean fields (for example, the ratio of standard deviations for vertical mean and eddy advection is 16/5). Contributions to potential temperature fluxes from solar radiation in the bottom of the lower entrainment zone and the top of the upper entrainment zone are negligible (not shown).

In this case study, the surface is warmer than the cloud, causing a net longwave warming at cloud base (0.97–1.14 km) (Fig. 9b). This warming is largely balanced by

Maintenance of Arctic stratocumulus

A. Solomon et al.

Title Page

Abstract

Introduction

Conclusions

References

Tables

Figures

◀

▶

◀

▶

Back

Close

Full Screen / Esc

Printer-friendly Version

Interactive Discussion



cooling from evaporation, however the cooling due to divergence of potential temperature fluxes causes a net cooling of -4 K day^{-1} . There is a relatively uniform cooling of -4 K day^{-1} within the mixed layer (Fig. 9a,b). Within the lower entrainment zone, mixing by turbulent horizontal and vertical fluxes tend to cancel.

5.3.3 Turbulent kinetic energy tendencies

TKE tendency terms are calculated following Eq. (5) and then averaged horizontally across the total square domain. The shear (S), buoyancy (B), TKE transport (T), and residual ($R = P + D$) terms are plotted in Fig. 10. The storage term is negligible so $R \approx S + B + T$. The gray shading in Fig. 10 marks the entrainment zones. The mean resolved TKE is approximately constant $0.4\text{--}0.5 \text{ m}^2 \text{ s}^{-2}$ within the mixed layer, decreasing to below $0.1 \text{ m}^2 \text{ s}^{-2}$ above 1.32 km and below 0.7 km.

Negative TKE tendencies due to buoyancy effects in the upper entrainment zone, associated with the temperature inversion, are largely balanced by TKE generation by the pressure transport term, as the dissipation contribution to R can only be negative. At the base of this upper entrainment zone, TKE is primarily produced by shear and is transported downward into the mixed layer. Within the mixed layer, TKE is produced by buoyancy effects resulting from radiative cooling above 1.15 km and evaporative cooling plus advection below 1.15 km (see Fig. 9). This buoyancy, combined with shear, produces TKE within the mixed layer, much of which is dissipated within the mixed layer. Buoyancy contributes to negative TKE tendencies near the bottom of the mixed-layer; however, this term is small relative to the transport of TKE from the top to the bottom of the mixed-layer. All TKE tendencies approach zero near the bottom of the mixed-layer.

5.3.4 Averaged water tendencies and mean fields

Vapor, liquid water, and ice tendencies, as well as mean vertical velocity, θ_e , vapor, and cloud water profiles averaged over the square domain in Fig. 6 and temporally averaged over the 90-min period are plotted in Fig. 11. Figure 11a shows the contribution of

Maintenance of Arctic stratocumulus

A. Solomon et al.

Title Page

Abstract

Introduction

Conclusions

References

Tables

Figures

◀

▶

◀

▶

Back

Close

Full Screen / Esc

Printer-friendly Version

Interactive Discussion



cloud water, cloud ice, and water vapor to the total water tendency. The layers marked with gray shading are entrainment zones defined based on the vertical structure of θ_e and detailed in the discussion above. Water vapor decreases throughout the upper entrainment zone, partially due to the condensation of cloud water resulting in positive cloud water tendencies above the mixed layer. Positive ice tendencies start just below the top of the upper entrainment zone. The loss of total water in the mixed layer is essentially independent of height, resulting from a loss of cloud water and water vapor above 1 km and vapor from 1 km to the base of the mixed layer. Within the cloud, liquid water evaporates and is advected downward. Below the lower entrainment zone, vapor increases due to sublimating ice precipitation, surface moisture fluxes and mean horizontal advection.

Figure 11b shows the average vertical velocity is a weak subsidence at and above cloud top of $-0.4 \pm 0.3 \text{ cm s}^{-1}$. A mean subsidence of up to -2.5 cm s^{-1} occurs within the mixed layer, with large variability. Weak upward motion occurs below the mixed layer. At the top of the upper entrainment zone, the mean vertical velocity goes to zero with relatively limited variability ($< \pm 0.5 \text{ cm s}^{-1}$). Vertical velocities in individual up- and downdrafts within the mixed layer are typically 100 times larger than these mean values. Twenty three percent of the vertically integrated cloud liquid water is located within the inversion (Fig. 11c). Maximum liquid water occurs at the water vapor minimum, which is at the inversion base. Significantly larger values of water vapor occur above and below the cloud layer.

Time series of the 15-min averaged water content tendencies in the upper entrainment zone and mixed layer are plotted in Fig. 12. A close compensation between cloud water and water vapor tendencies is seen in the upper entrainment zone, with the sum always resulting in a net loss of total water, with a rate between -50 to $-200 \text{ g m}^{-2} \text{ day}^{-1}$. The contribution of the ice tendency to the total water tendency in the upper entrainment zone is negligible. The inversion height remains at 1.3 km over the 90-min analysis period (results not shown). In the mixed layer, the large negative total water tendency is dominated by a loss of water vapor. Loss of cloud water has much

Maintenance of Arctic stratocumulus

A. Solomon et al.

Title Page

Abstract

Introduction

Conclusions

References

Tables

Figures



Back

Close

Full Screen / Esc

Printer-friendly Version

Interactive Discussion



less variability than water vapor, and contributes between -100 to $-500 \text{ g m}^{-2} \text{ day}^{-1}$ during each 15-min period to the total water tendency in the mixed layer. The ice tendency contributes positively to the total water tendency. The mixed layer base moves downward at a rate of 50 m h^{-1} over the 90-min analysis period (results not shown).

Water content tendencies are given by Eq. (4), where term Q_{2*} represents diabatic moistening or microphysics processes, including sedimentation, and the last two terms represent horizontal and vertical advective tendencies, respectively. Since advective tendencies in the model are formulated in flux form, the mean flow and eddy contributions to the advective tendency are calculated offline as:

$$\underbrace{\bar{u} \frac{\partial \bar{q}_*}{\partial x}}_{\text{UVM}} + \underbrace{\bar{v} \frac{\partial \bar{q}_*}{\partial y}}_{\text{WM}} + \underbrace{\bar{w} \frac{\partial \bar{q}_*}{\partial z}}_{\text{WM}} + \underbrace{\frac{(\overline{u'q'_*})_e - (\overline{u'q'_*})_w}{x_e - x_w} + \frac{(\overline{v'q'_*})_e - (\overline{v'q'_*})_w}{y_n - y_s}}_{\text{UVP}} + \underbrace{\frac{\partial (\overline{w'q'_*})}{\partial z}}_{\text{WP}} \approx \underbrace{\text{ADV}}_{\text{ADVECT}} \quad (6)$$

where ADV is the total advective tendency calculated in the model, \bar{u} , \bar{v} , \bar{w} , \bar{q}_* are 15-min averaged zonal wind, meridional wind, vertical wind, and water constituents, respectively, and $\overline{u'q'_*}$, $\overline{v'q'_*}$, $\overline{w'q'_*}$ are the resolved turbulent fluxes calculated from the total flux and mean fields. x_e, x_w, y_n, y_s are the zonal and meridional boundaries of the domain, with $x_e - x_w = y_n - y_s = 6.5 \text{ km}$. The notation below (Eq. 6) indicates the abbreviations used for the advection terms. The difference between the total tendency and the sum of the advective and microphysical tendencies is equal to subgrid-scale mixing plus diffusion, which are not represented in Eq. (4). This difference will be referred to as the residual (RES) hereafter. The residual is calculated using instantaneous total, advective, and microphysical tendencies output every minute. Layer budgets are calculated by vertically integrating Eqs. (4) and (6) from 0.82–1.24 km for the mixed layer and 1.24–1.3 km for the upper entrainment zone.

Total water content tendencies above the base of the lower entrainment zone are plotted in Figs. 13 and 14. The net contribution of microphysical processes to the total

Maintenance of Arctic stratocumulus

A. Solomon et al.

Title Page	
Abstract	Introduction
Conclusions	References
Tables	Figures
◀	▶
◀	▶
Back	Close
Full Screen / Esc	
Printer-friendly Version	
Interactive Discussion	



Discussion Paper | Discussion Paper | Discussion Paper | Discussion Paper | Discussion Paper

Maintenance of Arctic stratocumulus

A. Solomon et al.

[Title Page](#)[Abstract](#)[Introduction](#)[Conclusions](#)[References](#)[Tables](#)[Figures](#)[◀](#)[▶](#)[◀](#)[▶](#)[Back](#)[Close](#)[Full Screen / Esc](#)[Printer-friendly Version](#)[Interactive Discussion](#)

water tendency is equal to sedimentation because phase-change terms cancel for total water. Since total, advective and microphysical tendency terms averaged over every time step were not available for analysis, Fig. 13a shows these tendency terms averaged over instantaneous fields output every minute. The advect (flux) tendency term is the sum of the advective tendencies in Eq. (6), while advect is the exact advective tendency output from the model. The difference between the advect and advect (flux) curves is an estimate of the error in the post-processed advective tendencies relative to the tendencies output from the model, and is generally small throughout the profile.

At the top boundary of the upper entrainment zone there is a decrease in total water of $-1 \text{ g m}^{-3} \text{ day}^{-1}$ (Fig. 13a), with the dominant term being the vertical turbulent advection of water vapor (WP in Fig. 14b). Within the entrainment zone there is down gradient mixing of both water vapor and cloud liquid water such that turbulent vertical advection within the entrainment layer increases (decreases) cloud liquid water (water vapor) above 1.27 km and oppositely below (Fig. 14b,c). Tendencies due to subgrid-scale mixing (RES in figures) are of the same order as mean vertical advection for vapor in the upper entrainment zone. Sedimentation, which is the microphysics term in Figs. 13a and 14a because phase transitions conserve total water, is a maximum within the upper entrainment zone due to the fallout of primarily liquid water and some ice within the entrainment zone into the mixed layer. Liquid water is generated in the entrainment zone from condensation (Fig. 14c) and falls into the mixed layer (Fig. 13b). Ice is mixed into the entrainment zone from the mixed layer by turbulent eddies and then falls back down (Figs. 13b and 14d), with only a small amount of ice formation within the entrainment zone. At the lower boundary of the upper entrainment zone there is a positive (negative) tendency of water vapor (cloud liquid water) due to vertical turbulent fluxes. The vertical turbulent fluxes are balanced closely by condensation/evaporation and sedimentation.

From 1.1 km to the top of the mixed layer, total water tendency due to sedimentation and eddy vertical advection tend to cancel (Fig. 14a), such that the total tendency in the mixed layer is a drying of approximately $-2 \text{ g m}^{-3} \text{ day}^{-1}$ that is essentially independent

of height (Fig. 13a). Within the cloudy portion of the mixed layer, the largest tendency term is the increase (decrease) in water vapor (cloud liquid water) due to evaporation.

Figure 15a,b shows the vertical resolved turbulent ($\overline{w'q'_*}$) and mean ($\overline{wq_*}$) fluxes of water above the base of the lower entrainment zone, respectively. In Fig. 15b it is clearly seen that the vertical mean water vapor fluxes are an order of magnitude larger than the vertical mean cloud water and ice fluxes. This is due to large vertical mass fluxes that do not contribute to vertical mean advective tendencies of water vapor (WM in Fig. 14b). Figure 15b indicates that there is a mean larger-scale (larger than the 6.5×6.5 km square domain used in the analysis) circulation within the mixed layer and upper entrainment zone producing a horizontal mass flux into the upper entrainment zone and upper mixed layer, a downward mass flux within the mixed layer, and a horizontal mass flux out of the lower mixed layer. The largest vertical mean mass flux is located near the base of the cloud layer, which suggests that this larger-scale circulation is driven by the cloud layer itself. In order to isolate the vertical mean fluxes that contribute to the advection by the mean vertical velocity, the mean water vapor used to calculate the water vapor flux in Fig. 15b is modified by removing the vertically averaged mean water vapor between 0.7–1.4 km (modified fluxes plotted in Fig. 15c). This modified water vapor flux reduces the mass flux contribution to the vertical mean water vapor flux. Figure 15d shows the extent to which the mass flux contribution has been eliminated from the modified water vapor flux by comparing the advection of water vapor by the mean vertical velocity (WM in Fig. 14b) to the vertical derivative of the modified water vapor flux shown in Fig. 15c. Differences between the two curves in Fig. 15d indicate that the mean water vapor flux is overestimated near the top and bottom of the mixed layer.

Comparing Figs. 15a and 15c, it is seen that at the top of the upper entrainment zone both the turbulent and mean vertical fluxes are essentially equal to zero. Therefore, the decrease in total water by turbulent eddies in the upper part of the entrainment zone is primarily due to a downward transport of water vapor from below the top of the upper entrainment zone. In addition, the turbulent flux of total water at the top of the mixed

Maintenance of Arctic stratocumulus

A. Solomon et al.

Title Page

Abstract

Introduction

Conclusions

References

Tables

Figures

◀

▶

◀

▶

Back

Close

Full Screen / Esc

Printer-friendly Version

Interactive Discussion



layer is positive, primarily due to positive fluxes of cloud water and ice. The mean flux of total water is approximately equal to zero at the top of the mixed layer, with a positive flux of vapor balancing a negative flux of cloud water (Fig. 15c). The slightly negative total flux of total water at the base of the mixed layer is primarily due to a negative flux of water vapor by the mean flow, which is partially offset by a small positive turbulent vapor flux. However, its magnitude is about $-0.0003 \text{ g m}^{-2} \text{ s}^{-1}$, which is an order of magnitude smaller than the vertical flux due to the sedimentation of ice at the base of the mixed layer (results not shown), showing that the net flux of water through the base of the mixed layer is primarily due to sedimentation and not to mean or turbulent vertical motions.

5.3.5 Layer budgets

Following Curry et al. (1988), we calculate vertically integrated water content budgets in the mixed layer and upper entrainment zone with Eq. (6). Table 3 shows the contribution of advection and microphysics to the water content tendencies in the upper entrainment zone. Note that the microphysics term in the total water tendencies is equal to sedimentation. There is a net decrease in total water in the upper entrainment zone, i.e. sedimentation out is greater than net advection in. The upper entrainment zone loses $-99 \text{ g m}^{-2} \text{ day}^{-1}$ on average over the 90-min period. This rate varies from -30 to $-200 \text{ g m}^{-2} \text{ day}^{-1}$ (Fig. 12). This net loss of total water is produced through a daily net gain of 100 g m^{-2} of cloud water and a daily net loss of 203 g m^{-2} of water vapor. Because water vapor has no sedimentation, the daily loss of 379 g m^{-2} of water vapor due to microphysics implies a daily net gain of 379 g m^{-2} of liquid water due to condensation, assuming minimal ice formation. The daily gain of 208 g m^{-2} of q_c from microphysics then implies a daily sedimentation of 171 g m^{-2} of cloud water from the upper entrainment zone. Mean and eddy vertical advection produce a daily loss of 100 g m^{-2} of q_c , while they produce a gain of 181 g m^{-2} of water vapor. There is a minimal net gain of cloud ice in this zone, with the daily gain of 71 g m^{-2} due to lofting

Maintenance of Arctic stratocumulus

A. Solomon et al.

Title Page

Abstract

Introduction

Conclusions

References

Tables

Figures

◀

▶

◀

▶

Back

Close

Full Screen / Esc

Printer-friendly Version

Interactive Discussion



Maintenance of Arctic stratocumulus

A. Solomon et al.

Title Page

Abstract

Introduction

Conclusions

References

Tables

Figures

◀

▶

◀

▶

Back

Close

Full Screen / Esc

Printer-friendly Version

Interactive Discussion



by eddy vertical advection from the mixed layer below mostly offset by sedimentation such that the ice tendency is relatively neutral. A small amount of cloud ice is produced through phase changes (deposition, freezing; Fig. 13b). Hence, the water budget in the entrainment zone consists of a net loss of total water primarily due to condensation of liquid water, with a loss of 72 % of this liquid water to the mixed layer through sedimentation and vertical advection. The vertical profiles (Fig. 14) additionally show that water vapor is primarily redistributed from the top of the entrainment zone to the base of the entrainment zone by vertical mixing due to resolved eddies.

Table 4 shows the contribution of advection and microphysics to the water content tendencies integrated over the mixed layer from 0.82–1.24 km. The mixed layer loses $-696 \text{ g m}^{-2} \text{ day}^{-1}$ of water averaged over the 90-min period. The rate of depletion of total water from the mixed layer varies from -300 to $-950 \text{ g m}^{-2} \text{ day}^{-1}$, while the loss of cloud liquid water is $-281 \text{ g m}^{-2} \text{ day}^{-1}$ and ranges from -100 to $-450 \text{ g m}^{-2} \text{ day}^{-1}$ over the six 15-min periods. The mixed layer is $7\times$ deeper than the upper entrainment zone and loses $7\times$ as much water, with 43 % of this loss due to horizontal advection. Mean vertical advection, sedimentation, and upward transport by eddies each contribute between 15 % and 21 % of this loss. In the cloudy portion of the mixed layer, evaporation and collection (riming) reduces the cloud water at a rate of $-523 \text{ g m}^{-2} \text{ day}^{-1}$, while ice and water vapor both increase through these processes (Fig. 13b). A substantial amount of the water vapor increase is converted to cloud ice through deposition as well (i.e., the Bergeron process). There is also a substantial loss ($-136 \text{ g m}^{-2} \text{ day}^{-1}$) of cloud water due to mean horizontal advection and loss of water vapor due to mean vertical advection (Fig. 14b). Within the cloud in the mixed layer, sedimentation produces decreases of ice and smaller increases in liquid water (Fig. 13b). Below cloud base within the mixed layer, ice amounts increase weakly due to both sedimentation and vapor deposition, while weak losses of water vapor occur from all terms, including mean horizontal advection (Fig. 14b).

Looking at total water alone, it would be assumed that the cloud would dissipate due to the loss of water in both the upper entrainment zone and the mixed layer. However,

the transport of water vapor into the lower part of the upper entrainment zone is large enough to cause condensation that continually forms cloud water that is transported downward into the mixed layer. In the mixed layer, loss due to microphysics exceeds the transport of cloud water from the entrainment zone resulting in a continual net loss of cloud water.

5.4 Downdraft and updraft averages

Vapor, water and ice tendencies averaged over updrafts and downdrafts separately in the square domain and temporally averaged over the 90-min period are plotted in Fig. 16. Also shown in Fig. 16 are mean vertical velocity and θ_e profiles averaged over downdrafts and updrafts separately. Downdrafts are defined as gridpoints where the minimum vertical velocity within the cloud layer is less than -30 cm s^{-1} (see Fig. 16c). Updrafts are defined as gridpoints where the maximum vertical velocity within the cloud layer is greater than 20 cm s^{-1} (see Fig. 16d). Out of the total 16 900 gridpoints, approximately 3000–4000 gridpoints at a given time are classified as downdrafts and 4000–5000 gridpoints are classified as updrafts. These numbers are consistent with cloud dynamics forced by radiative cooling at cloud top, which result in narrower yet stronger downdrafts relative to updrafts. Vertical velocity above the cloud layer is approximately -0.4 cm s^{-1} in averages over updrafts and downdrafts. Figure 16a,b shows the contribution of cloud water, cloud ice, and water vapor to the downdraft and updraft total water tendencies, respectively. It is clearly seen that within the upper entrainment zone the decrease in water vapor and increase in cloud liquid water seen in the averages over the total domain in Fig. 11 only occur above downdrafts. Above updrafts, compensating tendencies of water vapor increases and liquid water losses are present. In mixed-layer downdrafts, cloud water decreases while water vapor, ice, and total water increase. These tendencies are qualitatively similar to the mean tendencies discussed earlier. Compensating effects occur in mixed-layer updrafts, where cloud water increases (within the cloud) while a decrease of water vapor, ice, and total water occurs throughout. Note that the cloud water increase in the updrafts occurs above the

Maintenance of Arctic stratocumulus

A. Solomon et al.

Title Page

Abstract

Introduction

Conclusions

References

Tables

Figures

◀

▶

◀

▶

Back

Close

Full Screen / Esc

Printer-friendly Version

Interactive Discussion



base of the cloud water decrease in the downdrafts, suggesting a modulation of cloud base height by the vertical motion.

The tendencies in water vapor and cloud water in updrafts and downdrafts in Fig. 16 are due to compensating large microphysics and advection tendencies that sum to a smaller residual (see Fig. 17). Within the cloud layer, in downdrafts, opposite vertical gradients of cloud liquid water and water vapor cause an increase (decrease) in cloud water (water vapor) due to advected moisture that evaporates (condenses), resulting in smaller residuals in water vapor and cloud liquid water with opposite tendencies (Fig. 17a,c). The average water vapor tendency due to microphysics in the cloud layer in downdrafts exceeds $30 \text{ g kg}^{-1} \text{ day}^{-1}$. Approximately the opposite is true in updrafts, though the advective and microphysical tendency magnitudes are smaller (Fig. 17b,d). The ice tendencies are dominated by the advective tendencies in both updrafts and downdrafts, while the sedimentation and total microphysics terms are quite small (Fig. 17e,f).

It is important to note that condensation occurs in the upper entrainment zone in both updrafts and downdrafts (Fig. 17a–d). This process of “radiative encroachment,” or forcing of direct condensation by cooling that cannot be balanced by convection, is a process that contributes to the positive cloud water tendency in the upper entrainment zone (Fig. 11). This process occurs because of the specific humidity inversion that is coincident with the temperature inversion. We also emphasize that this radiative condensational processes, occurring above both updrafts and downdrafts, is quite different from the adiabatic cooling process simultaneously producing condensation in the mixed layer updrafts as seen in Fig. 17b. Lastly, while in the mixed layer cloud liquid condensation and evaporation occur in updrafts and downdrafts, respectively, deposition on cloud ice occurs in both updrafts and downdrafts (i.e., the difference between the sedimentation and microphysics terms in Fig. 17e,f).

Maintenance of Arctic stratocumulusA. Solomon et al.

[Title Page](#)[Abstract](#)[Introduction](#)[Conclusions](#)[References](#)[Tables](#)[Figures](#)[◀](#)[▶](#)[◀](#)[▶](#)[Back](#)[Close](#)[Full Screen / Esc](#)[Printer-friendly Version](#)[Interactive Discussion](#)

6 Summary and discussion

In this paper we use high-resolution nested LES simulations to quantify the processes involved in the maintenance and persistence of a single-layer, decoupled AMPS that was observed near Barrow, Alaska during ISDAC on 8 April 2008. To focus on feedbacks within the inversion and cloud layer, all regions of open water were removed and surface conditions were specified as sea ice, i.e. observed conditions were only specified at the horizontal boundaries of the 25 km nest. It was found that removing the open water had a negligible impact on the cloud structure in the region of analysis. A mean temperature inversion of 6.5 K and humidity inversion of 0.4 g kg^{-1} with a base at 1.2 km was simulated in the LES at 20 Z, similar to the sounding taken at 17.6 Z that showed a mean temperature inversion of 5.0 K and humidity inversion of 0.5 g kg^{-1} with a base at 1.1 km.

The LES below 1.3 km is composed of five distinct layers; a turbulent surface layer, a stable layer from 200–600 m, a lower entrainment zone between 0.62–0.82 km, a cloud-driven mixed layer between 0.82–1.24 km, and a (partly) cloudy upper entrainment zone between 1.24–1.30 km. Different from subtropical stratocumulus-topped boundary layers, the inversion height remains at 1.3 km over the 90 min analysis period while the mixed layer base moves downward at a rate of 50 m h^{-1} . Another distinctly Arctic characteristic is that cloud water extends into the inversion layer.

Longwave radiative cooling peaks within the temperature inversion and upper entrainment zone but also extends 80 m down into the mixed layer, coincident with turbulent vertical potential temperature fluxes. The average potential temperature tendency due to longwave cooling at the top of the mixed layer is approximately -80 K day^{-1} . There is a relatively uniform cooling of -4 K day^{-1} within the mixed layer.

Buoyancy, shear, pressure transport, and TKE transport make significant contributions to the vertical distribution of TKE tendencies. In the upper entrainment zone, TKE production is dominated by pressure transport and shear but limited by buoyancy. At the top of the mixed layer shear is the dominant production term. Moving down into the

Maintenance of Arctic stratocumulus

A. Solomon et al.

Title Page

Abstract

Introduction

Conclusions

References

Tables

Figures

◀

▶

◀

▶

Back

Close

Full Screen / Esc

Printer-friendly Version

Interactive Discussion



mixed layer, shear remains important along with buoyancy production. TKE is advected downward to the base of the mixed layer where TKE production by the other terms is small. All production terms become small below the mixed layer.

At the top boundary of the upper entrainment zone there is a decrease in total water of $-1 \text{ g m}^{-3} \text{ day}^{-1}$ primarily due to eddy vertical advection of water vapor. Within the entrainment zone there is down gradient mixing by turbulent eddies that causes an upward (downward) transport of cloud liquid water (water vapor) above the liquid water maximum, and oppositely below. The increase (decrease) in water vapor (cloud liquid water) due to turbulent fluxes in the lower part of the entrainment zone is closely balanced by a decrease (increase) by condensation and sedimentation, with sedimentation exceeding advection of total water by $2 \text{ g m}^{-3} \text{ day}^{-1}$ at the lower boundary. The upper entrainment zone loses an average of $-99 \text{ g m}^{-2} \text{ day}^{-1}$ of total water to the mixed layer.

The mixed layer loses total water at a rate of $-696 \text{ g m}^{-2} \text{ day}^{-1}$. This tendency is primarily due to horizontal advection by the mean flow, while $-387 \text{ g m}^{-2} \text{ day}^{-1}$ of the total water loss is approximately equally divided between loss due to turbulent vertical fluxes, loss due to mean vertical advection, and sedimentation (Table 4). Neglecting the tendencies due to the mean horizontal wind, the loss of cloud liquid water is due to microphysical processes, with this loss counteracted primarily by mean vertical advection at the top of the mixed layer. Turbulent and mean fluxes of total water at the top of the mixed layer are positive and larger than fluxes at the base.

The average loss of cloud water from the upper entrainment zone plus mixed layer system is $-181 \text{ g m}^{-2} \text{ day}^{-1}$, or $7.5 \text{ g m}^{-2} \text{ h}^{-1}$. However, over this 90-min period the upper entrainment zone gains cloud water while continually losing total water. This is due to the continuous source of water vapor provided to the cloud layer by turbulent down gradient mixing and condensation forced by radiative cooling that cannot be balanced by convection. For an initial liquid water path of 50 g m^{-2} , assuming no change in the dynamical balance, a cloud could persist at this rate for 6.7 h. The net loss of cloud water is only 23% of the loss of total water, i.e. the mixed layer plus entrainment zone

Maintenance of Arctic stratocumulus

A. Solomon et al.

Title Page

Abstract

Introduction

Conclusions

References

Tables

Figures

◀

▶

◀

▶

Back

Close

Full Screen / Esc

Printer-friendly Version

Interactive Discussion



is losing vapor 3.5 times faster than it is losing cloud water.

Interestingly, mean subsidence above the upper entrainment zone is of the same order as mean subsidence in subtropical cloud-topped boundary layers (see Wood and Bretherton, 2004) and LES simulations of AMPS (see Klein et al., 2009). However, mean subsidence goes to zero right at the top of the upper entrainment zone, resulting in no net vertical flux of water into the upper entrainment zone. Essentially all of the vertical transport of water into the mixed layer initiates in the upper entrainment zone.

This study has shown that sedimentation plays a dominant role in the vertical transport and depletion of water from a decoupled AMPS cloud system. This sedimentation is due to both the gravitational settling of liquid water and the continuous precipitation of ice. In this model study, the production of ice is underestimated relative to the retrievals. It is unclear what the impact of ice production closer to the retrievals would have on the simulation. For example, in subtropical boundary layers, sedimentation removes water near cloud top resulting in less entrainment of dry, warm air and a more persistent cloud (Ackerman et al., 2004; Bretherton et al., 2007). Sedimentation in AMPS at cloud top may have the opposite effect, as entrainment of dry air does not occur. Also, the production of more ice would cause more condensational heating to balance the longwave cooling and thereby modify the vertical motions in the mixed layer. In addition, more ice production may cause more moistening of the surface layer.

In both updrafts and downdrafts the vertical velocity above the cloud layer is approximately -0.4 cm s^{-1} . The decrease in water vapor and increase in cloud liquid water in the upper entrainment zone occurs primarily above downdrafts. Above updrafts, there is an increase in water vapor at this height. Similar compensating tendencies between water vapor, cloud liquid water, and cloud ice water above updrafts and downdrafts are seen in the mixed layer.

The results of this nested LES study form a relatively simple conceptual model of decoupled AMPS where the essential structures and processes are:

1. A humidity inversion at cloud top that provides a weak source of moisture to the cloud layer via entrainment caused by cloud-generated turbulence. This continual

Maintenance of Arctic stratocumulus

A. Solomon et al.

Title Page

Abstract

Introduction

Conclusions

References

Tables

Figures

◀

▶

◀

▶

Back

Close

Full Screen / Esc

Printer-friendly Version

Interactive Discussion



**Maintenance of
Arctic stratocumulus**

A. Solomon et al.

[Title Page](#)[Abstract](#)[Introduction](#)[Conclusions](#)[References](#)[Tables](#)[Figures](#)[I◀](#)[▶I](#)[◀](#)[▶](#)[Back](#)[Close](#)[Full Screen / Esc](#)[Printer-friendly Version](#)[Interactive Discussion](#)

down gradient transport of water vapor into the cloud layer supports its persistence.

2. The primary and necessary source of energy for the system is longwave radiative cooling at, and near, cloud top. Radiative cooling does at least two things: 1) Forces direct condensation in non-buoyant parcels near cloud top that are inside the temperature and moisture inversions. 2) Forces turbulence and buoyancy-driven overturning of parcels within a mixed-layer associated with the cloud layer, with additional condensation occurring in the updraft portions of this mixed layer.
3. The primary transport of total water from the entrainment zone into the mixed layer is via sedimentation of liquid water. Ice precipitation is the primary net sink of condensed mass from the cloud mixed layer.

We speculate that collapse of the system occurs when the moisture source above the cloud is exhausted (i.e., supply rate of moisture due to entrainment is less than the sedimentation rate of condensate out of the cloud mixed layer for a long enough time) and/or condensed liquid water drops below its threshold for efficient emission causing radiative cooling, and therefore buoyant overturning, to diminish (see Morrison et al., 2011 for a discussion on this point).

We also acknowledge that the descriptions of the budgets and processes are almost solely based on the model representation of the AMPS for this one case. Hence, the model configuration and physics have significant impacts on the results. Both the configuration and the physics impacting the cloud have been carefully chosen to produce the most realistic evolution possible. However, one deficiency is clearly the apparent underestimation of cloud ice by the model. Another deficiency is the apparently too strong surface turbulence, perhaps due to a poor representation of the surface conditions, although the cloud still remains decoupled. Future observational and modeling work should obtain detailed observations to verify the processes described here, especially those within the upper entrainment zone and the upper portion of the mixed

layer, improve model deficiencies, explore the generality of these results, and attempt to understand the processes modulating the coupling of AMPS with surface forcing.

Acknowledgement. This research was supported by the Office of Science (BER), US Department of Energy (DE-FG01-05ER63965) and National Science Foundation (ARC-1023366). Any opinions, findings and conclusions or recommendations expressed in this material are those of the authors and do not necessarily reflect the views of the sponsors. HM acknowledges partial funding from US DOE ARM DE-FG02-08ER64574, and the NSF Science and Technology Center for Multiscale Modeling of Atmospheric Processes (CMMAP), managed by Colorado State University under cooperative agreement ATM-0425247. Observational data used in this study were provided by the Department of Energy's Atmospheric Radiation Measurement Program. ECMWF datasets used as boundary conditions for the model simulations were downloaded from the Research Data Archive, which is maintained by the Computational and Information Systems Laboratory at the National Center for Atmospheric Research. The National Center for Atmospheric Research is sponsored by the National Science Foundation.

References

- Abdul-Razzak, H. and Ghan, S. J.: A parameterization of aerosol activation. 2. Multiple aerosol types, *J. Geophys. Res.*, 105(D5), 6837–6844, 2000.
- Ackerman, A. S., Kirkpatrick, M. P., Stevens, D. E., and Toon, O. B.: The impact of humidity above stratiform clouds on indirect aerosol climate forcing, *Nature*, 432, 1014–1017, 2004.
- Albrecht, B. A., Penc, R. S., and Schubert, W. H.: An observational study of cloud-topped mixed layers, *J. Atmos. Sci.*, 42, 800–822, 1985.
- Albrecht, B. A., Jensen, M. P., and Syrett, W. J.: Marine boundary layer structure and fractional cloudiness, *J. Geophys. Res.*, 100, 14209–14222, 1995.
- Bretherton, C. S., Blossey, P. N., and Uchida, J.: Cloud droplet sedimentation, entrainment efficiency, and subtropical stratocumulus albedo, *Geophys. Res. Lett.*, 34, L03813, doi:10.1029/2006GL027648, 2007.
- Brost, R. A., Wyngaard, J. C., and Lenschow, D. H.: Marine stratocumulus layers. Part II: Turbulence budgets, *J. Atmos. Sci.*, 39, 818–836, 1982.
- Chen, F. and Dudhia, J.: Coupling an advanced land-surface/hydrology model with the Penn

Maintenance of Arctic stratocumulus

A. Solomon et al.

Title Page

Abstract

Introduction

Conclusions

References

Tables

Figures

◀

▶

◀

▶

Back

Close

Full Screen / Esc

Printer-friendly Version

Interactive Discussion



**Maintenance of
Arctic stratocumulus**A. Solomon et al.

[Title Page](#)[Abstract](#)[Introduction](#)[Conclusions](#)[References](#)[Tables](#)[Figures](#)[◀](#)[▶](#)[◀](#)[▶](#)[Back](#)[Close](#)[Full Screen / Esc](#)[Printer-friendly Version](#)[Interactive Discussion](#)

State/NCAR MM5 modeling system. Part I: Model description and implementation, *Mon. Weather Rev.*, 129, 569–585, 2001.

Collins, W. D. Rasch, P. J., Boville, B. A., Hack, J. J., Mccaa, J. R., Williamson, D. L., and Briegleb, B. P.: Description of the NCAR Community Atmosphere Model (CAM 3.0), NCAR Technical Note, NCAR/TN-464+STR, 226 pp., 2004.

Curry, J. A., Ebert, E. E., and Herman, G. F.: Mean and turbulence structure of the summertime Arctic cloudy boundary layer, *Q. J. Roy. Meteorol. Soc.*, 114, 715–746, 1988.

Curry, J. A., Randall, D., Rossow, W. B., and Schramm, J. L.: Overview of arctic cloud and radiation characteristics, *J. Climate*, 9, 1731–1764, 1996.

Curry, J. A., Hobbs, P. V., King, M. D., Randall, D. A., Minnis, P., Isaac, G. A., Pinto, J. O., Uttal, T., Bucholtz, A., Cripe, D. G., Gerber, H., Fairall, C. W., Garrett, T. J., Hudson, J., Intrieri, J. M., Jakob, C., Jensen, T., Lawson, P., Marcotte, D., Nguyen, L., Pilewskie, P., Rangno, A., Rogers, D. C., Strawbridge, K. B., Valero, F. P. J., Williams, A. G., and Wylie, D.: FIRE Arctic clouds experiment, *B. Am. Meteorol. Soc.*, 81, 5–30, 2000.

Deardorff, J. W.: Prediction of convective mixed-layer entrainment for realistic capping inversion structure, *J. Atmos. Sci.*, 36, 424–436, 1979.

Deardorff, J. W.: Cloud top entrainment instability, *J. Atmos. Sci.*, 37, 131–147, 1980.

Dyer, A. J. and Hicks, B. B.: Flux-gradient relationships in the constant flux layer, *Q. J. Roy. Meteorol. Soc.*, 96, 715–721, 1970.

Garratt, J. R.: *The Atmospheric Boundary Layer*, Cambridge University Press, Cambridge, UK, 316 pp., 1992.

Harrington, J., Reisin, T., Cotton, W. R., and Kreidenweis, S. M.: Exploratory cloud resolving simulations of boundary layer Arctic stratus. Part II: Transition-season clouds. *Atmos. Res.*, 51, 45–75, doi:10.1016/S0169-8095(98)00098-2, 1999.

Hong, S.-Y., Noh, Y., and Dudhia, J.: A new vertical diffusion package with an explicit treatment of entrainment processes, *Mon. Weather Rev.*, 134, 2318–2341, 2006.

Jiang, H. J., Feingold, G., Cotton, W. R., and Duynkerke, P. G.: Large-eddy simulations of entrainment of cloud condensation nuclei into the Arctic boundary layer: May 18, 1998, FIRE/SHEBA case study, *J. Geophys. Res.*, 106, 15113–15122, 2001.

Klein, S. A., McCoy, R., Morrison, H., Ackerman, A., Avramov, A., de Boer, G., Chen, M., Cole, J., DelGenio, A. D., Falk, M., Foster, M., Fridlind, A., Golaz, J.-C., Hashino, T., Harrington, J., Hoose, C., Khairoutdinov, M., Larson, V., Liu, X., Luo, Y., McFarquhar, G., Menon, S., Negggers, R., Park, S., von Salzen, K., Schmidt, J. M., Sednev, I., Shipway, B., Shupe, M.,

Maintenance of Arctic stratocumulus

A. Solomon et al.

Title Page

Abstract

Introduction

Conclusions

References

Tables

Figures

◀

▶

◀

▶

Back

Close

Full Screen / Esc

Printer-friendly Version

Interactive Discussion



Spangenberg, D., Sud, Y., Turner, D., Veron, D., Walker, G., Wang, Z., Wolf, A., Xie, S., Xu, K.-M., Yang, G., and Zhang, G.: Intercomparison of model simulations of mixed-phase clouds observed during the ARM Mixed-Phase Arctic Cloud Experiment. I: Single-layer cloud, *Q. J. Roy. Meteorol. Soc.*, 135, 979–1002, 2009.

5 McFarquhar, G. M., Ghan, S., Verlinde, J., Korolev, A., Strapp, J. W., Schmid, B., Tomlinson, J. M., Wolde, M., Brooks, S. D., Cziczo, D., Dubey, M. K., Fan, J., Flynn, C., Gultepe, I., Hubbe, J., Gilles, M. K., Laskin, A., Lawson, P., Leaitch, W. R., Liu, P., Liu, X., Lubin, D., Mazzoleni, C., Macdonald, A.-M., Moffet, R. C., Morrison, H., Ovchinnikov, M., Shupe, M. D., Turner, D. D., Xie, S., Zelenyuk, A., Bae, K., Freer, M., and Glen, A.: Indirect and Semi-Direct
10 Aerosol Campaign (ISDAC): the impact of Arctic aerosols on clouds, *B. Am. Meteorol. Soc.*, 92, 183–201, doi:10.1175/2010BAMS2935.1, 2011.

Morrison, H. and Pinto, J. O.: Mesoscale modeling of springtime Arctic mixed-phase stratiform clouds using a new two-moment bulk microphysics scheme, *J. Atmos. Sci.*, 62, 3683–3704, 2005.

15 Morrison, H. and Pinto, J. O.: Intercomparison of bulk cloud microphysics schemes in mesoscale simulations of springtime Arctic mixed-phase stratiform clouds, *Mon. Weather Rev.*, 134, 1880–1900, 2006.

Morrison, H., Thompson, G., and Tatarskii, V.: Impact of cloud microphysics on the development of trailing stratiform precipitation in a simulated squall line: comparison of one- and two-moment schemes, *Mon. Weather Rev.*, 137, 991–1007, doi:10.1175/2008MWR2556.1, 2009.

Morrison, H., Pinto, J. O., Curry, J. A., and McFarquhar, G. M.: Sensitivity of modeled arctic mixed-phase stratocumulus to cloud condensation and ice nuclei over regionally varying surface conditions, *J. Geophys. Res.*, 113, D05203, doi:10.1029/2007JD008729, 2008.

25 Morrison, H., Zuidema, P., Ackerman, A. S., Avramov, A., de Boer, G., Fan, J., Fridlind, A. M., Hashino, T., Harrington, J. Y., Luo, Y., Mikhail Ovchinnikov, M., and Shipway, B.: Intercomparison of cloud model simulations of Arctic mixed-phase boundary layer clouds observed during SHEBA, J.A.M.E.S. accepted, 2011.

Nicholls, S.: The dynamics of stratocumulus: aircraft observations and comparisons with a mixed layer model, *Q. J. Roy. Meteorol. Soc.*, 110, 783–820, 1984.

30 Norris, J. R.: Low cloud type over the ocean from surface observations. Part I: Relationship to surface meteorology and the vertical distribution of temperature and moisture, *J. Climate*, 11, 369–382, 1998.

**Maintenance of
Arctic stratocumulus**A. Solomon et al.

[Title Page](#)[Abstract](#)[Introduction](#)[Conclusions](#)[References](#)[Tables](#)[Figures](#)[◀](#)[▶](#)[◀](#)[▶](#)[Back](#)[Close](#)[Full Screen / Esc](#)[Printer-friendly Version](#)[Interactive Discussion](#)

- Paulson, C. A.: The mathematical representation of wind speed and temperature profiles in the unstable atmospheric surface layer, *J. Appl. Meteor.*, 9, 857–861, 1970.
- Pinto, J. O.: Autumnal mixed-phase cloudy boundary layers in the Arctic, *J. Atmos. Sci.*, 55, 2016–2038, doi:10.1175/1520-0469(1998)055<2016:AMPCBL>2.0.CO;2, 1998.
- 5 Prenni, A. J., Harrington, J. Y., Tjernström, M., DeMott, P. J., Avramov, A., Long, C. N., Kreidenweis, S. M., Olsson, P. Q., and Verlinde, J.: Can ice-nucleating aerosols affect Arctic seasonal climate?, *B. Amer. Meteorol. Soc.*, 88, 541–550, 2007.
- Randall, D. A.: Conditional instability of the first kind upside-down, *J. Atmos. Sci.*, 37, 125–130, 1980.
- 10 Sedlar, J. and Tjernström, M.: Stratiform cloud-inversion characterization during the Arctic melt season, *Bound.-Layer Meteorol.*, 132, 455–474, 2009.
- Sedlar, J., Shupe, M. D., and Tjernström, M.: On the relationship between thermodynamic structure and cloud top, and its climate significance in the Arctic, submitted, *J. Climate*, 2011.
- 15 Shupe, M. D.: A ground-based multiple remote-sensor cloud phase classifier, *Geophys. Res. Lett.*, 34, L2209, doi:10.1029/2007GL031008, 2007.
- Shupe, M. D.: Clouds at Arctic atmospheric observatories. Part II: Thermodynamic phase characteristics, *J. Appl. Meteorol. Clim.*, 50, 645–661, 2011.
- Shupe, M. D., Matrosov, S. Y., and Uttal, T.: Arctic mixed-phase cloud properties derived from surface-based sensors at SHEBA, *J. Atmos. Sci.*, 63, 697–711, 2006.
- 20 Shupe, M. D., Kollias, P., Poellot, M., and Eloranta, E.: On deriving vertical air motions from cloud radar Doppler spectra, *J. Atmos. Ocean. Tech.*, 25, 547–557, 2008a.
- Shupe, M. D., Kollias, P., Persson, P. O. G., and McFarquhar, G. M.: Vertical motions in Arctic mixed-phase stratiform clouds, *J. Atmos. Sci.*, 65, 1304–1322, 2008b.
- 25 Solomon, A., Morrison, H., Persson, O., Shupe, M., and Bao, J.-W.: Investigations of microphysical parameterizations of snow and ice in Arctic clouds during M-PACE through model-observations comparison, *Mon. Weather Rev.*, 137, 3110–3128, 2009.
- Skamarock, W. C., Klemp, J. B., Dudhia, J., Gill, D. O., Barker, D. M., Duda, M. G., Huang, X.-Y., Wang, W., and Powers, J. G.: A description of the Advanced Research WRF version 3. NCAR Tech. Note NCAR/TN-475+STR, 113 pp., 2008.
- 30 Stevens, B., Cotton, W. R., Feingold, G., and Moeng, C.-H.: Large-eddy simulations of strongly precipitating, shallow, stratocumulus-topped boundary layers, *J. Atmos. Sci.*, 55, 3616–3638, 1998.

Maintenance of Arctic stratocumulus

A. Solomon et al.

Title Page

Abstract

Introduction

Conclusions

References

Tables

Figures

◀

▶

◀

▶

Back

Close

Full Screen / Esc

Printer-friendly Version

Interactive Discussion



Tjernström, M., Leck, C., Persson, P. O. G., Jensen, M. L., Oncley, S. P., and Targino, A.: The summertime Arctic atmosphere: meteorological measurements during the Arctic Ocean Experiment 2001, *B. Am. Meteorol. Soc.*, 85, 1305–1321, 2004.

5 Turner, D. D., Clough, S. A., Liljegren, J. C., Clothiaux, E. E., Cady-Pereira, K., and Gaus-
tad, K. L.: Retrieving precipitable water vapor and liquid water path from Atmospheric Ra-
diation Measurement (ARM) program's microwave radiometers, *IEEE Trans. Geosci. R.*, 45,
3680–3690, 2007.

Webb, E. K.: Profile relationships: the log-linear range, and extension to strong stability, *Q. J. Roy. Meteorol. Soc.*, 96, 67–90, 1970.

10 Wood, R. and Bretherton, C. S.: Boundary layer depth, entrainment, and decoupling in the
cloud-capped subtropical and tropical marine boundary layer, *J. Climate*, 17, 3576–3588,
2004.

Wyant, M. C., Bretherton, C. S., Rand, H. A., and Stevens, D. E.: Numerical simulations and
a conceptual model of the stratocumulus to trade cumulus transition, *J. Atmos. Sci.*, 54,
15 168–192, 1997.

Zhang, D.-L. and Anthes, R. A.: A high-resolution model of the planetary boundary layer–
sensitivity tests and comparisons with SESAME-79 data, *J. Appl. Meteor.*, 21, 1594–1609,
1982.

20 Zhu, P., Albrecht, B. A., Ghate, V. P., and Zhu, Z.: Multiple-scale simulations of stratocumulus
clouds, *J. Geophys. Res.*, 115, D23201, doi:10.1029/2010JD014400, 2010.

Maintenance of Arctic stratocumulus

A. Solomon et al.

Title Page

Abstract

Introduction

Conclusions

References

Tables

Figures

◀

▶

◀

▶

Back

Close

Full Screen / Esc

Printer-friendly Version

Interactive Discussion



Table 1. Packages used in WRF model setup.

Radiation package	National Center for Atmospheric Research Community Atmospheric Model longwave and shortwave radiation package. The longwave code allows for interactions with resolved clouds and cloud fractions (see Collins et al., 2004 for complete details).
Surface layer physics package	Monin-Obukhov with Carlson-Boland viscous sub-layer and standard similarity functions following Paulson (1970) and Dyer and Hicks (1970). Surface exchange coefficients for heat, moisture, and momentum computed following Webb (1970). Four stability regimes are defined following Zhang and Anthes (1982).
Land surface package	Noah Land Surface Model; the unified NCEP/NCAR/AFWA scheme with soil temperature and moisture in four layers, fractional snow cover and frozen soil physics (see Chen and Dudhia, 2001, for complete details).
Planetary boundary layer mixing package	Yonsei University scheme (non-local-K scheme with explicit entrainment layer and parabolic K profile in unstable mixed layers) in 6 and 18 km grids (see Hong et al., 2006 for complete details).

Maintenance of Arctic stratocumulus

A. Solomon et al.

Table 2. Variables and constants used in this study.

c_p	Specific heat at constant pressure = $1.003 \times 10^3 \text{ J kg}^{-1} \text{ K}^{-1}$
T	Temperature (K)
g	Gravitational acceleration = 9.81 m s^{-1}
z	Height (m)
L	Latent heat of condensation = $2.555 \times 10^6 \text{ J kg}^{-1}$
L_s	Latent heat of freezing = $2.898 \times 10^6 \text{ J kg}^{-1}$
P	Pressure (hPa)
P_0	Standard reference pressure = 1000 hPa
ρ	Density (kg m^{-3})
θ	Potential temperature (K)
θ_0	Reference state potential temperature (K)
t	Time (s)
R	Specific gas constant = $287 \text{ J kg}^{-1} \text{ K}^{-1}$

Title Page

Abstract

Introduction

Conclusions

References

Tables

Figures

◀

▶

◀

▶

Back

Close

Full Screen / Esc

Printer-friendly Version

Interactive Discussion



Maintenance of Arctic stratocumulus

A. Solomon et al.

Table 3. Mean (\pm one standard deviation) contribution of advection and microphysics to the time and horizontally averaged water content tendencies in the upper entrainment zone, in units of $\text{g m}^{-2} \text{day}^{-1}$. Advection by the mean flow is calculated from 15-min averaged fields. Eddies are defined as deviations from the 15-min averages. Total* is the sum of advection terms plus microphysics and is not exactly equal to the total tendency due to errors incurred by calculating the advection terms offline (see discussion of Fig. 13).

Upper entrainment zone	Mean horizontal advection	Eddy horizontal advection	Mean vertical advection	Eddy vertical advection	Micro-physics	Total*
Total water	-11 ± 45	-6 ± 3	34 ± 54	117 ± 14	-233 ± 10	-99 ± 85
Cloud water	-5 ± 77	-3 ± 4	-78 ± 33	-22 ± 64	208 ± 29	100 ± 152
Water vapor	-2 ± 111	-3 ± 6	113 ± 88	68 ± 45	-379 ± 28	-203 ± 226
Cloud ice	-4 ± 3	$+0 \pm 0$	-0 ± 1	71 ± 16	-62 ± 13	5 ± 3

Title Page

Abstract

Introduction

Conclusions

References

Tables

Figures

◀

▶

◀

▶

Back

Close

Full Screen / Esc

Printer-friendly Version

Interactive Discussion



Maintenance of Arctic stratocumulus

A. Solomon et al.

Table 4. Mean (\pm one standard deviation) contribution of advection and microphysics to the time and horizontally averaged water content tendencies in the mixed layer, in units of $\text{g m}^{-2} \text{ day}^{-1}$. Advection by the mean flow is calculated from 15-min averaged fields. Eddies are defined as deviations from the 15-min averages. Total* is the sum of advection terms plus microphysics and is not exactly equal to the total tendency due to errors incurred by calculating the advection terms offline (see discussion of Fig. 13).

Mixed layer	Mean horizontal advection	Eddy horizontal advection	Mean vertical advection	Eddy vertical advection	Micro-physics	Total*
Total water	-301 ± 192	-8 ± 6	-141 ± 74	-101 ± 25	-145 ± 49	-696 ± 256
Cloud water	-136 ± 110	-6 ± 3	363 ± 158	21 ± 64	-523 ± 169	-281 ± 137
Water vapor	-140 ± 295	3 ± 4	-484 ± 217	-56 ± 33	222 ± 185	-455 ± 341
Cloud ice	-24 ± 73	-5 ± 5	-21 ± 14	-65 ± 13	156 ± 23	41 ± 87

[Title Page](#)
[Abstract](#)
[Introduction](#)
[Conclusions](#)
[References](#)
[Tables](#)
[Figures](#)
[I◀](#)
[▶I](#)
[◀](#)
[▶](#)
[Back](#)
[Close](#)
[Full Screen / Esc](#)
[Printer-friendly Version](#)
[Interactive Discussion](#)

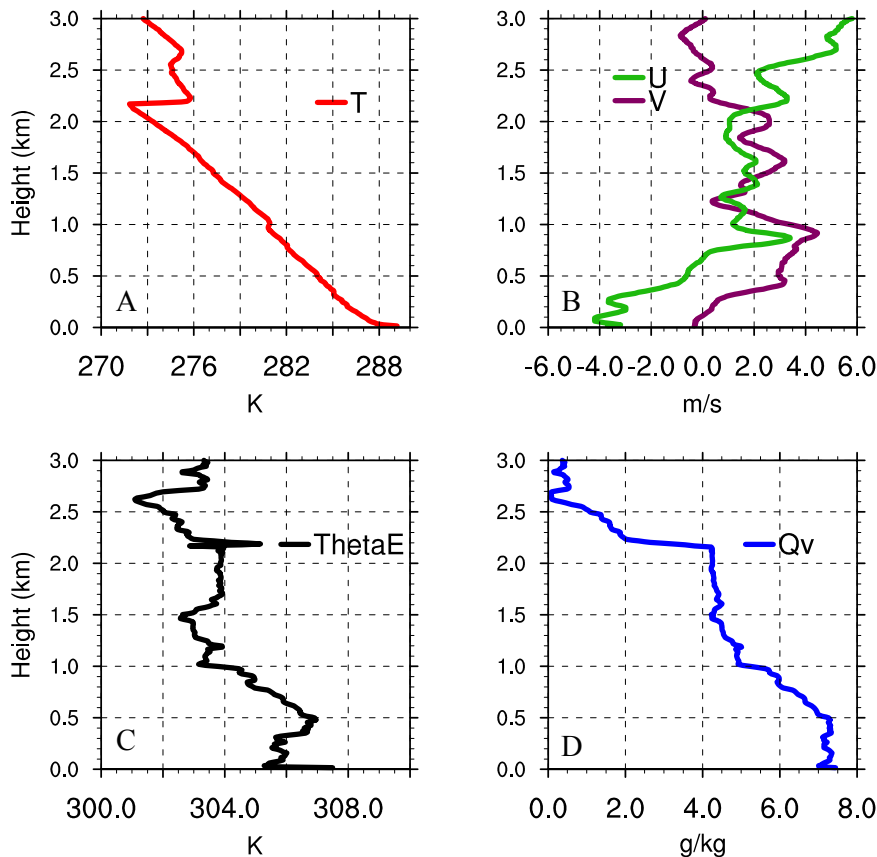



Fig. 1. Sounding of decoupled subtropical stratocumulus at 17:28Z 17 April 2010 over Graciosa Island, Azores, Portugal (39.13° N, 28.94° W). **(A)** Temperature, in units of K. **(B)** Horizontal winds, in units of m s^{-1} . **(C)** Equivalent potential temperature, in units of K. **(D)** Specific humidity, in units of g kg^{-1} .

Maintenance of
Arctic stratocumulus

A. Solomon et al.

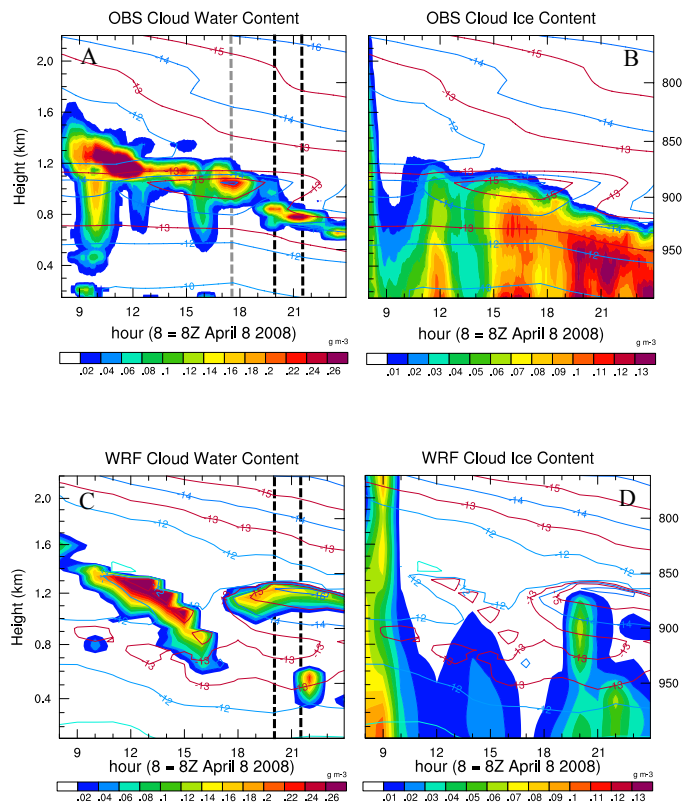


Fig. 2. Cloud liquid and ice water content, in g m^{-3} , at Barrow, Alaska from 8–24 Z 8 April 2008. One-hour running mean liquid water (**A**) and ice (**B**) output from retrievals. Hourly output of liquid water (**C**) and ice (**D**) from WRF 1 km nest. Temperature interpolated from soundings at 4.4 Z and 17.6 Z, in $^{\circ}\text{C}$, overlaid with contours. Note -13°C and -15°C contours are red to highlight inversions. Black dashed lines in (**A**) and (**C**) indicate the validation period. The gray dashed line in (**A**) indicates the time of the sounding.

Title Page

Abstract

Introduction

Conclusions

References

Tables

Figures

◀

▶

◀

▶

Back

Close

Full Screen / Esc

Printer-friendly Version

Interactive Discussion



**Maintenance of
Arctic stratocumulus**

A. Solomon et al.

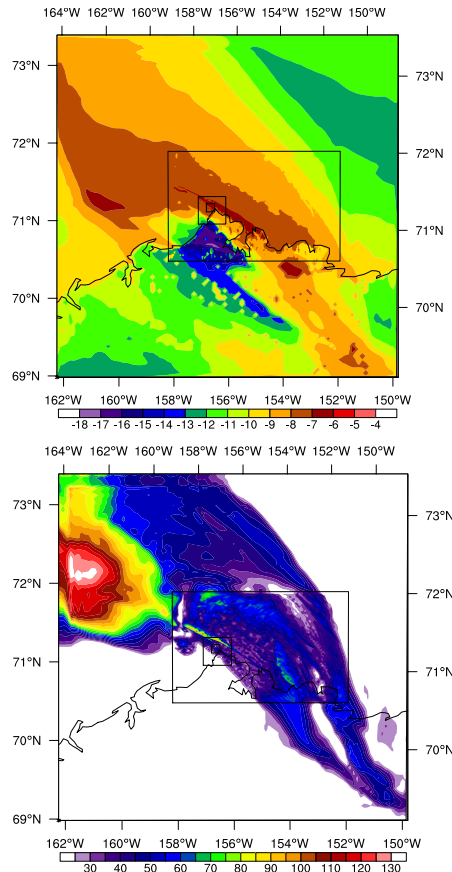


Fig. 3. Surface skin temperature (top) and liquid water path (bottom), in units of $^{\circ}\text{C}$ and g m^{-2} , respectively, at 20 Z 8 April 2008 for the 50 m, 200 m, 1 km and 5 km nests. Barrow, Alaska is located directly to the east of the 50 m nest southeast corner.

[Title Page](#)[Abstract](#)[Introduction](#)[Conclusions](#)[References](#)[Tables](#)[Figures](#)[◀](#)[▶](#)[◀](#)[▶](#)[Back](#)[Close](#)[Full Screen / Esc](#)[Printer-friendly Version](#)[Interactive Discussion](#)

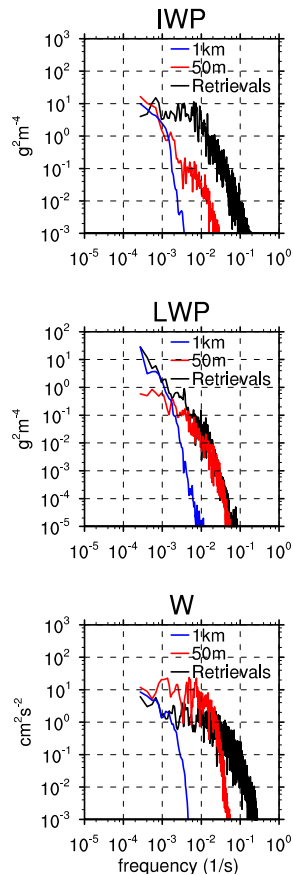


Fig. 4. IWP (top), LWP (middle), and W (bottom) spectra at Barrow for the 2 h period 20–22 Z 8 April 2008 from retrievals (black), 1 km nest (blue) and 50 m nest (red), in units of $\text{g}^2 \text{m}^{-4}$, $\text{g}^2 \text{m}^{-4}$, and $\text{cm}^2 \text{s}^{-2}$, respectively.

Maintenance of Arctic stratocumulus

A. Solomon et al.

Title Page	
Abstract	Introduction
Conclusions	References
Tables	Figures
◀	▶
◀	▶
Back	Close
Full Screen / Esc	
Printer-friendly Version	
Interactive Discussion	



Maintenance of Arctic stratocumulus

A. Solomon et al.

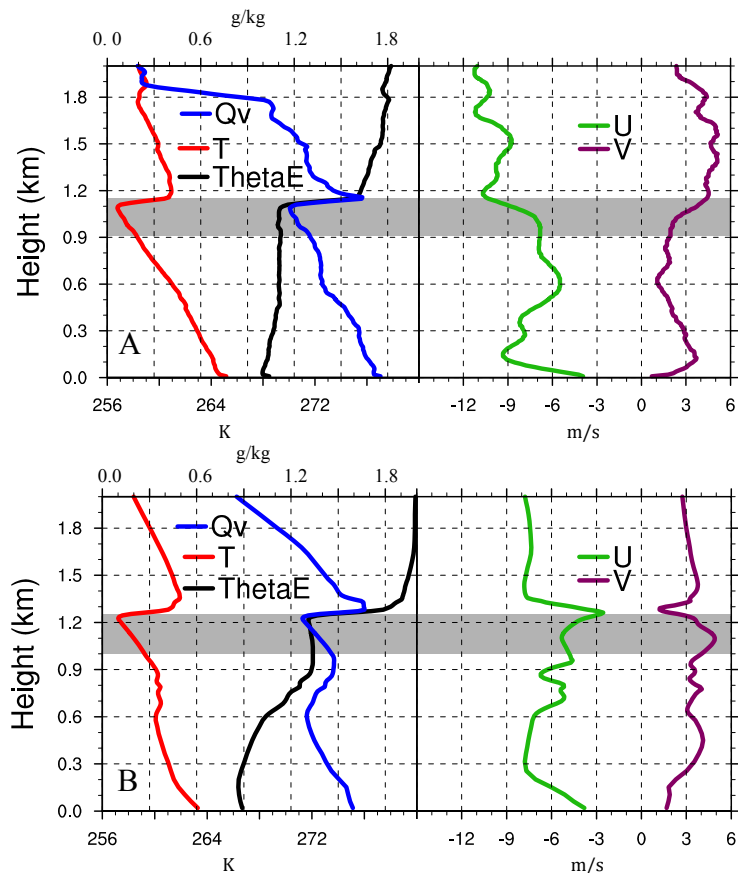


Fig. 5. Soundings of mid-day decoupled stratocumulus at Barrow, Alaska. **(A)** Measured 17.6 Z 8 April 2008 at (71.33° N, 156.61° W). **(B)** 50 m LES simulation 20 Z 8 April 2008 at (71.33° N, 156.91° W). Gray shading marks the extent of the cloud layer.

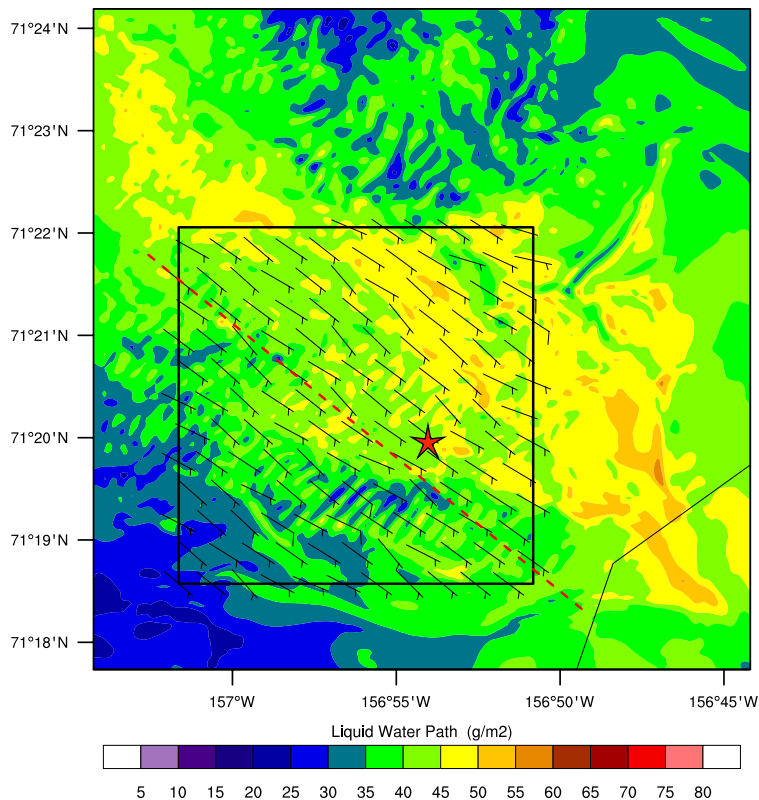


Fig. 6. Liquid water path and winds at maximum liquid water level, in units of g m^{-2} and m s^{-1} , respectively, on 20 Z 8 April 2008 for the 50 m nest. Barrow, Alaska is located directly to the east of the red star. The square marks the region used to make total, downdraft, and updraft averages (130×130 grid points). The red star marks the location of the vertical profiles plotted in Fig. 5. The red dashed line marks the diagonal slice plotted in Fig. 7. Thin black lines in the lower right outline the Alaskan coastline.

Maintenance of Arctic stratocumulus

A. Solomon et al.

Title Page	
Abstract	Introduction
Conclusions	References
Tables	Figures
◀	▶
◀	▶
Back	Close
Full Screen / Esc	
Printer-friendly Version	
Interactive Discussion	



Maintenance of Arctic stratocumulus

A. Solomon et al.

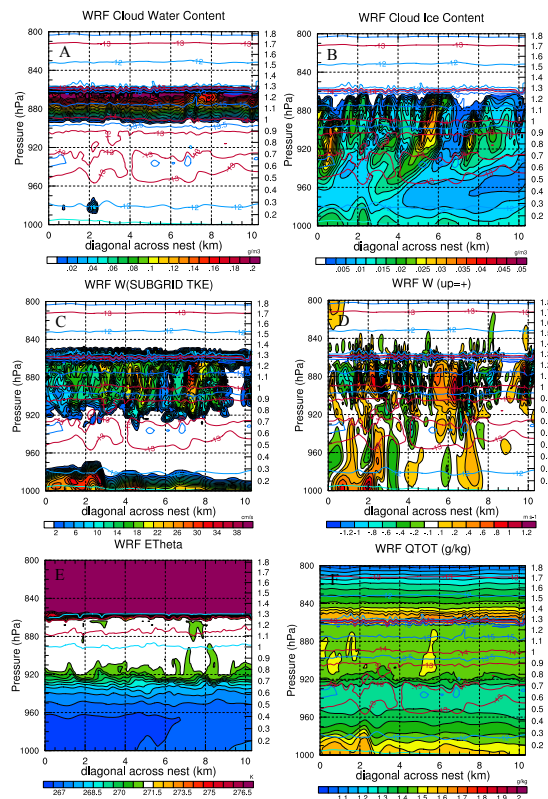


Fig. 7. Vertical structure at 20 Z along mean cloud layer wind from 50 m nest. **(A)** Cloud water, in units of g kg^{-1} . **(B)** Cloud ice, in units of g kg^{-1} . **(C)** Subgrid w , in units of cm s^{-1} . **(D)** Vertical velocity, in units of m s^{-1} . **(E)** Equivalent potential temperature, in units of K. Red (blue) lines are contours of $q_c = 0.12(0.01) \text{ g m}^{-3}$ to identify the max (min) of the cloud layer. **(F)** Total water, in units of g kg^{-1} . Isotherms are shown with colored contour lines in all figures except **(E)**.

Title Page

Abstract

Introduction

Conclusions

References

Tables

Figures

◀

▶

◀

▶

Back

Close

Full Screen / Esc

Printer-friendly Version

Interactive Discussion



Maintenance of Arctic stratocumulus

A. Solomon et al.

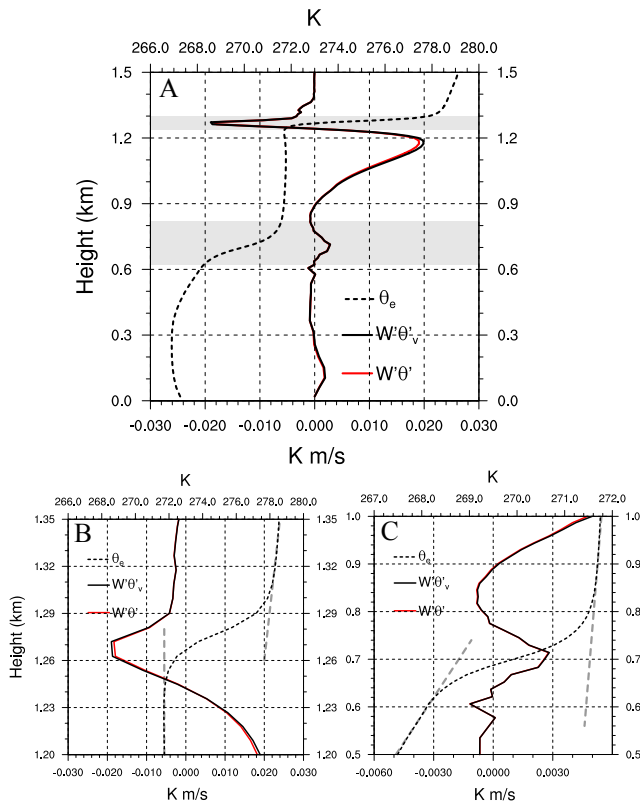


Fig. 8. Buoyancy fluxes averaged over total cloud domain, where black (red) lines show $\overline{W'\theta'_v}$ ($\overline{W'\theta'}$) and equivalent potential temperature (θ_e) is shown with a dashed line, in units of K m s^{-1} and K, respectively. **(A)** Surface to 1.5 km. Entrainment zones indicated with gray shading. **(B)** Cloud top entrainment zone. **(C)** Below mixed layer entrainment zone. Long dashed gray lines show constant θ_e slopes used to estimate the depth of the entrainment zones: 1.24–1.3 km = 60 m at cloud top and 0.62–0.82 km = 200 m below mixed layer.

Title Page

Abstract

Introduction

Conclusions

References

Tables

Figures

◀

▶

◀

▶

Back

Close

Full Screen / Esc

Printer-friendly Version

Interactive Discussion



Maintenance of Arctic stratocumulus

A. Solomon et al.

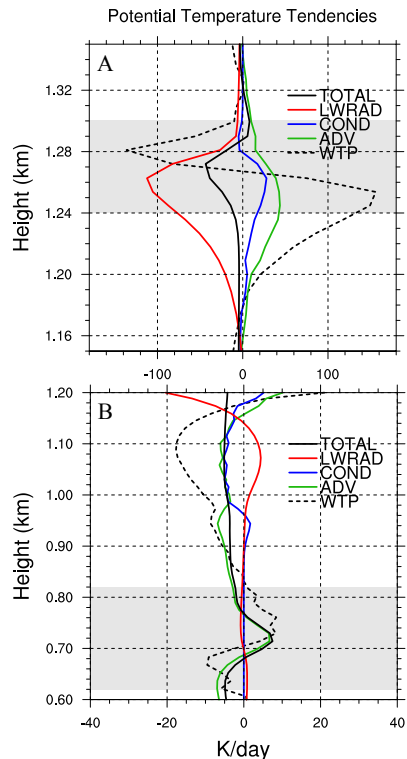


Fig. 9. Potential temperature tendencies averaged in the total cloud domain, in units of K day^{-1} . **(A)** The upper region of the mixed layer and cloud top entrainment zone. **(B)** Mixed layer and lower entrainment zone. Tendencies plotted are total advection (TOTAL, black), condensation/evaporation (COND, blue), longwave cooling (LWRAD, red), total tendency (ADV, green), and vertical eddy advection (WTP, black dash). Tendencies are horizontally averaged across the square domain and then temporally averaged over the 20:00 Z–21:29 Z period. Note change in scale between **(A)** and **(B)**. Entrainment zones indicated with gray shading.

Title Page

Abstract

Introduction

Conclusions

References

Tables

Figures

◀

▶

◀

▶

Back

Close

Full Screen / Esc

Printer-friendly Version

Interactive Discussion



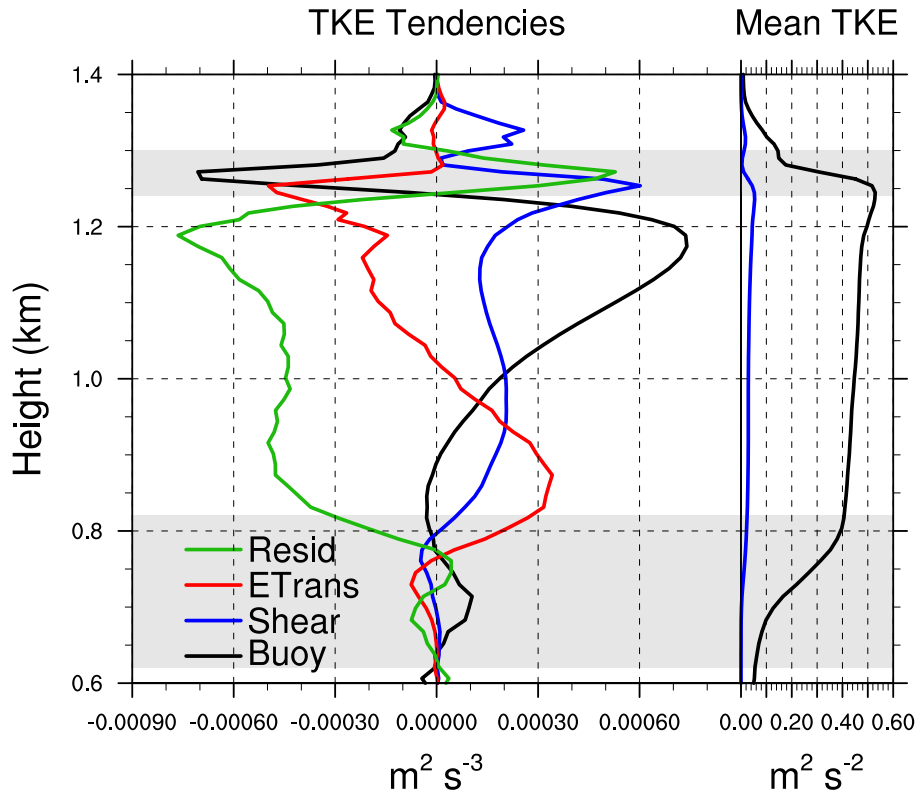


Fig. 10. Horizontally and temporally averaged turbulent kinetic energy (TKE). (Left) Resolved TKE tendencies in units of $\text{m}^2 \text{s}^{-3}$. Residual = pressure transport plus dissipation. (Right) Mean resolved (black) and subgrid (blue) TKE, in units of $\text{m}^2 \text{s}^{-2}$. Entrainment zones indicated with gray shading.

Maintenance of Arctic stratocumulus

A. Solomon et al.

Title Page

Abstract Introduction

Conclusions References

Tables Figures

◀ ▶

◀ ▶

Back Close

Full Screen / Esc

Printer-friendly Version

Interactive Discussion



Maintenance of Arctic stratocumulus

A. Solomon et al.

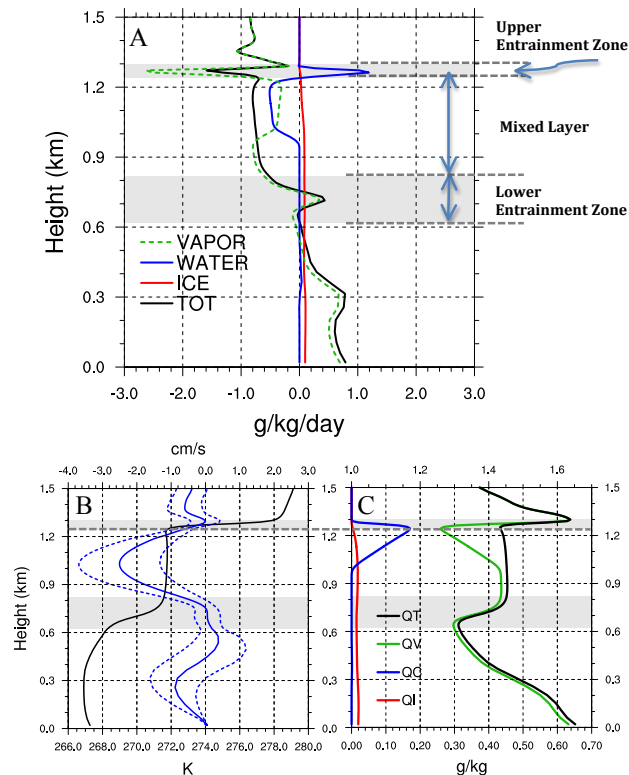


Fig. 11. Tendencies averaged over total cloud domain calculated from 15-min averages. Entrainment zones indicated with gray shading. **(A)** Cloud water, vapor, ice, and total water tendencies, in units of $\text{g kg}^{-1} \text{ day}^{-1}$. Gray dash lines denote boundaries of cloud top entrainment zone, mixed layer, lower entrainment zone. Positive (negative) indicates water gained (lost) by the layer. **(B)** Mean resolved vertical velocity (blue, dash lines are \pm one standard deviation) and equivalent potential temperature in black, in units of cm s^{-1} and K, respectively. **(C)** Mean total water, cloud liquid water, cloud ice water, and water vapor, in units of g kg^{-1} .

Maintenance of Arctic stratocumulus

A. Solomon et al.

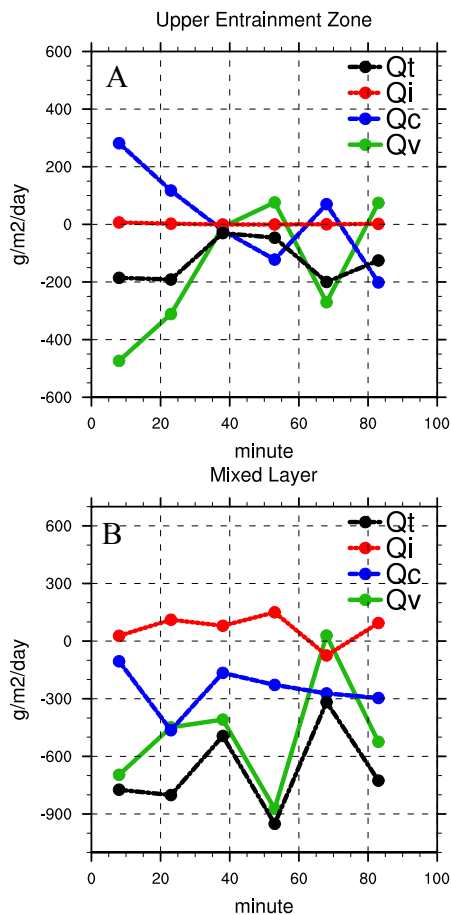


Fig. 12. Time series of 15-min averaged water content tendencies from 20:00 Z–21:29 Z in upper entrainment zone (A) and mixed layer (B), in units of g m⁻² day⁻¹.

Title Page

Abstract Introduction

Conclusions References

Tables Figures

◀ ▶

◀ ▶

Back Close

Full Screen / Esc

Printer-friendly Version

Interactive Discussion



Maintenance of Arctic stratocumulus

A. Solomon et al.

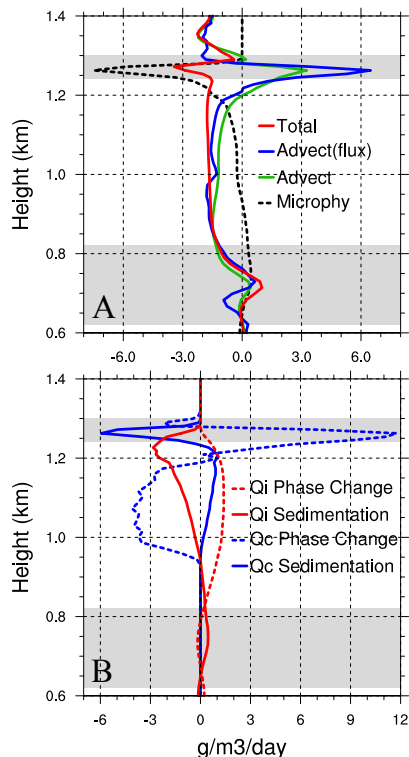


Fig. 13. (A) Processes that contribute to 15-min averaged total water content tendencies above the surface layer for the total cloud domain, in units of $\text{g m}^{-3} \text{day}^{-1}$. Note the net contribution due to microphysics for total water (Microphy) is equal to sedimentation, as condensational terms cancel. “Advect(flux)” is the total flux estimated using Eq. (6). “Advect” is the total advection output from the model. “Total” is the total water tendency. Entrainment zones indicated with gray shading. **(B)** Cloud liquid water and ice microphysical tendencies divided into contributions due to phase change and sedimentation, in units of $\text{g m}^{-3} \text{day}^{-1}$.

Title Page

Abstract

Introduction

Conclusions

References

Tables

Figures

◀

▶

◀

▶

Back

Close

Full Screen / Esc

Printer-friendly Version

Interactive Discussion



Maintenance of Arctic stratocumulus

A. Solomon et al.

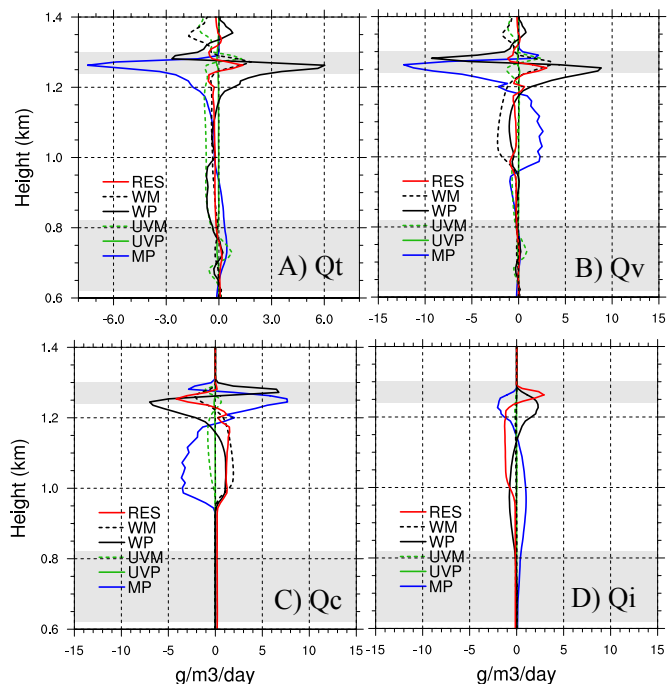


Fig. 14. Processes that contribute to 15-min averaged water content tendencies above the surface layer for the total cloud domain, in units of $\text{g m}^{-3} \text{day}^{-1}$. Note the net contribution due to microphysics for total water in **(A)** is equal to sedimentation, as condensational terms cancel. The residual is equal to subgrid scale mixing plus diffusion. Mean advection terms (denoted with WM, UVM) are calculated by horizontally averaging tendencies. Horizontal eddy advection (UVP) is calculated as the divergence of fluxes across the domain. Vertical eddy advection (WP) is the divergence of the vertical eddy flux. Note change in scale in **(A)**. Entrainment zones indicated with gray shading. **(A)** Total water. **(B)** Water vapor. **(C)** Cloud liquid water. **(D)** Cloud ice water.

Title Page

Abstract

Introduction

Conclusions

References

Tables

Figures

◀

▶

◀

▶

Back

Close

Full Screen / Esc

Printer-friendly Version

Interactive Discussion



Maintenance of
Arctic stratocumulus

A. Solomon et al.

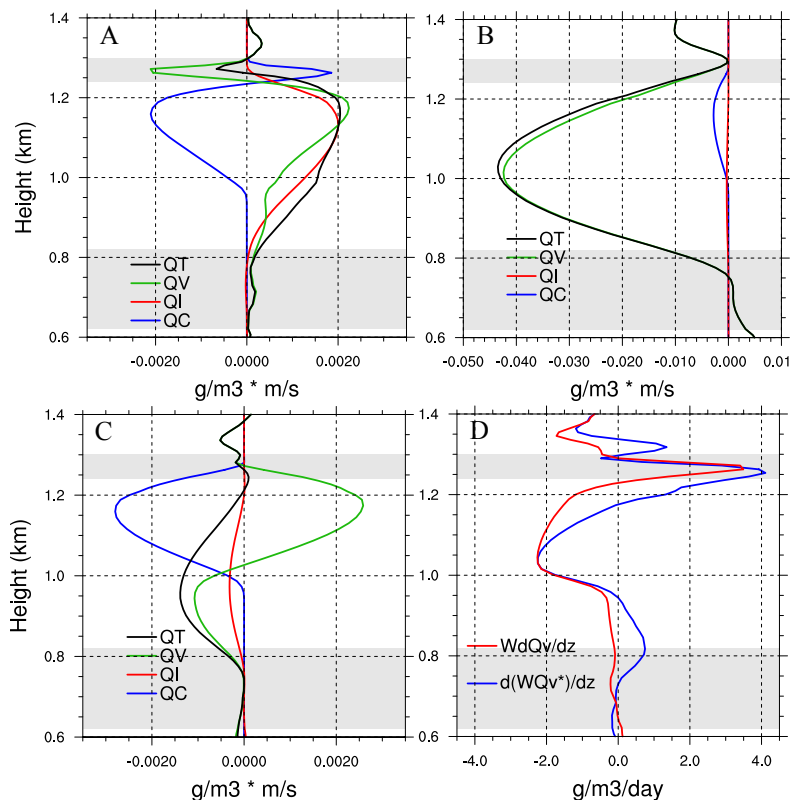


Fig. 15. Horizontally and temporally averaged vertical water content fluxes, in units of $g\ m^{-3}\ m\ s^{-1}$. Entrainment zones indicated with gray shading. **(A)** Eddy fluxes. **(B)** Mean fluxes. **(C)** Mean fluxes as in **(B)** except mean water vapor vertically averaged between 0.7–1.4 km is removed before calculating the mean water vapor flux. **(D)** Vertical derivative of modified mean water vapor flux (WQv^*) from **(C)** compared to the water vapor tendency due to advection by the mean vertical velocity (WM in Fig. 14b).

Title Page

Abstract

Introduction

Conclusions

References

Tables

Figures

◀

▶

◀

▶

Back

Close

Full Screen / Esc

Printer-friendly Version

Interactive Discussion



Maintenance of Arctic stratocumulus

A. Solomon et al.

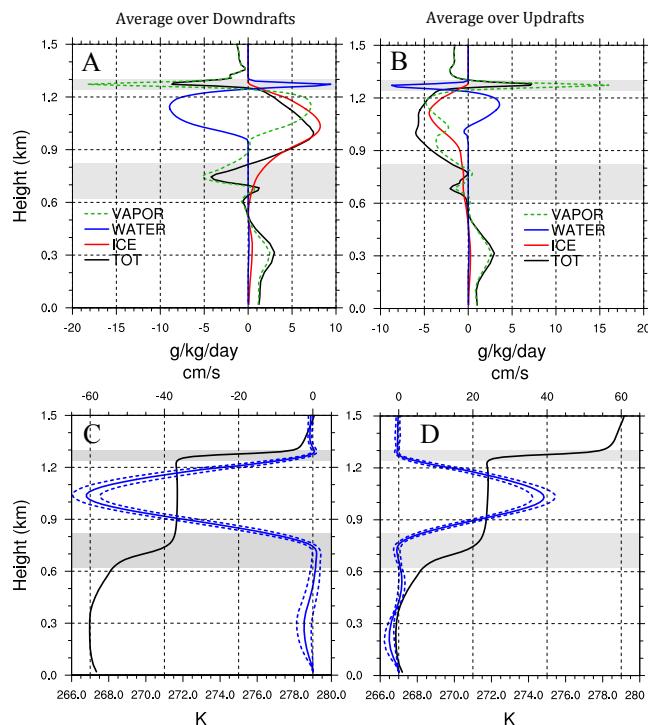


Fig. 16. (A) Liquid, vapor, ice and total water mixing ratio tendencies averaged over downdrafts in the cloud domain, in units of $\text{g kg}^{-1} \text{day}^{-1}$. (B) Liquid, vapor, ice and total water tendencies averaged over updrafts, in units of $\text{g kg}^{-1} \text{day}^{-1}$. (C) Downdraft mean resolved vertical velocity (blue, \pm one standard deviation of 1-min averages dashed) and equivalent potential temperature (black), in units of cm s^{-1} and K, respectively. (D) Updraft mean resolved vertical velocity (blue, \pm one standard deviation of 1-min averages dashed) and equivalent potential temperature (black), in units of cm s^{-1} and K, respectively. Entrainment zones indicated with gray shading.

Title Page

Abstract

Introduction

Conclusions

References

Tables

Figures

◀

▶

◀

▶

Back

Close

Full Screen / Esc

Printer-friendly Version

Interactive Discussion

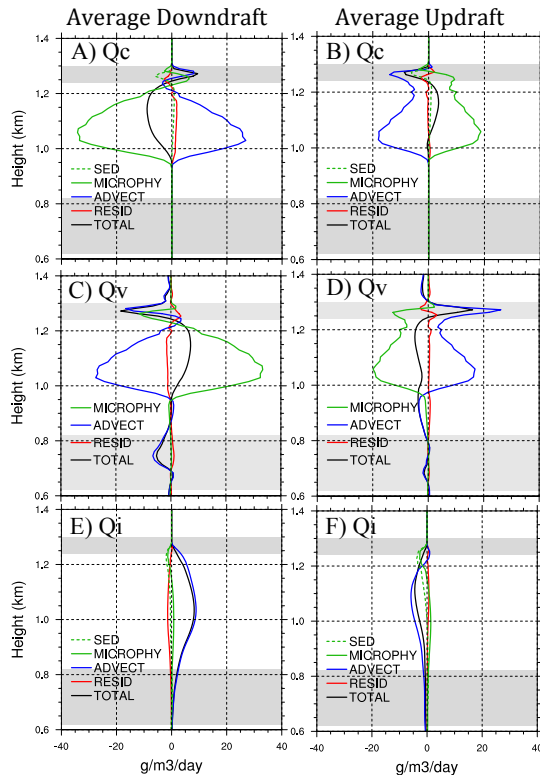


Fig. 17. Processes that contribute to water content tendencies between 0.6–1.4 km averaged over downdrafts and updrafts, in units of $\text{g m}^{-3} \text{ day}^{-1}$. **(A)** Cloud liquid water tendencies in downdrafts. **(B)** Cloud liquid water tendencies in updrafts. **(C)** Water vapor tendencies in downdrafts. **(D)** Water vapor tendencies in updrafts. **(E)** Cloud ice water tendencies in downdrafts. **(F)** Cloud ice water tendencies in updrafts. The contribution of sedimentation to the microphysical tendencies is shown with a green dashed line in **(A)**, **(B)**, **(E)**, **(F)**. Entrainment zones indicated with gray shading.

Maintenance of Arctic stratocumulus

A. Solomon et al.

Title Page

Abstract Introduction

Conclusions References

Tables Figures

◀ ▶

◀ ▶

Back Close

Full Screen / Esc

Printer-friendly Version

Interactive Discussion

